

1

2 **Seasonal cycles and trends of water budget components in 18**  
3 **river basins across the Tibetan Plateau: a multiple datasets**  
4 **perspective**

5

6 Wenbin Liu<sup>a</sup>, Fubao Sun<sup>a\*</sup>, Yanzhong Li<sup>a</sup>, Guoqing Zhang<sup>b,c</sup>,

7 Yan-Fang Sang<sup>a</sup>, Jiahong Liu<sup>d</sup>, Hong Wang<sup>a</sup>, Peng Bai<sup>a</sup>

8

9 <sup>a</sup>Key Laboratory of Water Cycle and Related Land Surface Processes, Institute of Geographic  
10 Sciences and Natural Resources Research, Chinese Academy of Sciences, Beijing 100101, China

11 <sup>b</sup>Key Laboratory of Tibetan Environmental Changes and Land Surface Processes, Institute of  
12 Tibetan Plateau Research, Chinese Academy of Sciences, Beijing 100101, China

13 <sup>c</sup>CAS Center for Excellent in Tibetan Plateau Earth Sciences, Beijing 100101, China

14 <sup>d</sup>Key Laboratory of Simulation and Regulation of Water Cycle in River Basin, China Institute of  
15 Water Resources and Hydropower Research, Beijing 100038, China

16

17 **Submitted to:** Hydrology and Earth System Sciences

18 **Corresponding Author:** Dr. Fubao Sun ([Sunfb@igsnr.ac.cn](mailto:Sunfb@igsnr.ac.cn)), from the Key Laboratory of Water  
19 Cycle and Related Land Surface Processes, Institute of Geographic Sciences and Natural  
20 Resources Research, Chinese Academy of Sciences (No. A11, Datun Road, Chaoyang District,  
21 Beijing 100101, China)

22 **Email Addresses for other authors:** Wenbin Liu ([liuwb@igsnr.ac.cn](mailto:liuwb@igsnr.ac.cn)), Yanzhong Li  
23 ([liy.14b@igsnr.ac.cn](mailto:liy.14b@igsnr.ac.cn)), Guoqing Zhang ([guoqing.zhang@itpcas.ac.cn](mailto:guoqing.zhang@itpcas.ac.cn)), Yan-fang Sang  
24 ([sangyf@igsnr.ac.cn](mailto:sangyf@igsnr.ac.cn)), Jiahong Liu ([liujh@iwhr.com](mailto:liujh@iwhr.com)), Hong Wang ([wanghong@igsnr.ac.cn](mailto:wanghong@igsnr.ac.cn)),  
25 Peng Bai ([baip.11b@igsnr.ac.cn](mailto:baip.11b@igsnr.ac.cn))

26

27

2016/11/25

28

29 **Highlights**

- 30 ● Monthly basin-wide ET was calculated through water balance considering the
- 31 impacts of glacier and water storage change
- 32 ● Water budget components and trends for 18 river basins over the TP were
- 33 evaluated
- 34 ● Uncertainties were discussed from multiple dataset perspective

35

36 **Abstract.** The dynamics of water budget over the Tibetan Plateau (TP) are not fully  
37 understood so far due to the lack of quantitative observations of the land surface water  
38 cycle. Here, we investigated the seasonal cycles and trends of water budget  
39 components, e.g., precipitation, runoff and evapotranspiration (ET), in 18 TP basins  
40 using multi-source datasets during the period 1982-2011. A two-step bias correction  
41 procedure was applied to calculate the basin-wide ET considering the influences of  
42 glacier and water storage change. The results indicated that precipitation, which  
43 mainly concentrated during June-October (varied among different monsoons impacted  
44 basins), is the major contributor to the runoff in the TP basins. The basin-wide snow  
45 water equivalent (SWE) was relatively higher from mid-autumn to spring for most TP  
46 basins. The water cycles intensified under a global warming in most basins except for  
47 the upper Yellow and Yalong Rivers, which were significantly influenced by the  
48 weakening East Asian monsoon. Consistent with the climate warming and moistening  
49 in the TP and western China, the aridity index (PET/P) in most basins decreased. The  
50 results highlighted the usefulness of integrating the multi-source data (e.g., in situ  
51 observations, remote sensing products, reanalysis, land surface model simulations and  
52 climate model outputs) for hydrological applications in the data-sparse regions and  
53 could be beneficial for understanding the water and energy budgets, sustainable  
54 management of water resources under a warming climate in the harsh and the  
55 data-sparse Tibetan Plateau.

56

## 57 **1 Introduction**

58 As the highest plateau in the globe (the average elevation is higher than 4000 meters

59 above the sea level), the Tibetan Plateau (TP, also called “the roof of the world” or  
60 “the third Pole”) is one of the most vulnerable region under a warming climate and is  
61 subjected to strong interactions among atmosphere, hydrosphere, biosphere and  
62 cryosphere in the earth system (Duan and Wu, 2006; Yao et al., 2012; Liu W. et al.,  
63 2016b). It also serves as the “Asian water tower” from which many major Asian rivers  
64 such as Yellow river, Yangtze river, Brahmaputra river, Mekong river, Indus river, etc.,  
65 originate. It provides a vital water resource to support hundreds of millions of people  
66 in China and the surrounding countries (Immerzell et al., 2010; Zhang et al., 2013).  
67 Knowledge about the water budgets and their responses to the changing environment  
68 is thus crucial for understanding the hydrological regimes and for sustainable water  
69 resources management as well as environmental protection in this special region  
70 (Yang et al., 2014; Chen et al., 2015).

71

72 The TP is also known as a typical data-sparse mountain region which brings great  
73 challenges to hydrological and related land surface studies (Zhang et al., 2007; Li F. et  
74 al., 2013; Liu X. et al., 2016). For example, since the 1950s, totally 750 stations have  
75 been established over China by the Chinese Meteorological Administration (CMA),  
76 among which only less than 80 stations are distributed over the plateau (Wang and  
77 Zeng, 2012). They are primary sparse and unevenly located at relatively low elevation  
78 regions, focus only on the meteorological variables and lack of other land surface  
79 observations such as evapotranspiration, snow water equivalent and latent heat fluxes,  
80 etc.. In addition, long-term consecutive observations of river discharge, snow depth,  
81 lake depth and glacier melts in the TP are also absent (Akhta et al., 2009; Ma et al.,  
82 2016). Therefore, the insights of water balance over various TP river basins located at  
83 different monsoon-dominant regions are still unclear so far (Cuo et al., 2014; Xu et al.,

84 2016). One way to overcome this limitation is to install more instruments to measure  
85 the in situ water budgets (Yang et al., 2013; Zhou et al., 2013; Ma et al., 2015), but it  
86 is extremely expensive to maintain long-term observations at basin or regional scales.  
87 Another workaround is to simulate basin-wide water budgets through physical-based  
88 land surface models at several large river basins forced with remote sensing data and  
89 large-scale gridded meteorological forcing datasets (Bookhagen and Burbank, 2010;  
90 Xue et al., 2013; Zhang et al., 2013; Cuo et al., 2015; Zhou et al., 2015; Wang et al.,  
91 2016). However, it is still difficult to use land surface models to multiple basins  
92 especially to the relatively smaller ones under complex terrains due to the lack of  
93 adequate data for model calibration and validation (Li F. et al., 2014).

94  
95 A number of global (or regional) datasets for water budget components have been  
96 released recently including remote sensing-based retrievals (Tapley et al., 2004;  
97 Zhang et al., 2010; Long et al., 2014; Zhang Y. et al., 2016), land surface model (LSM)  
98 simulations (Rui, 2011), reanalysis outputs (Berrisford et al., 2011; Kobayashi et al.,  
99 2015) and gridded forcing data interpolated from the in situ observations (Harries et  
100 al., 2014). For example, there are many products for terrestrial evapotranspiration (ET)  
101 such as GLEAM\_E (Global Land surface Evaporation: the Amsterdam Methodology,  
102 Miralles et al., 2011a), MTE\_E (a product integrated the point-wise ET observation at  
103 FLUXNET sites with geospatial information extracted from surface meteorological  
104 observations and remote sensing in a machine-learning algorithm, Jung et al., 2010 ),  
105 LSM-simulated ETs from Global Land Data Assimilation System version 2  
106 (GLDAS-2) with different land surface schemes (Rodell et al., 2004), ETs from  
107 Japanese 55-year reanalysis (JRA55\_E), the ERA-Interim global atmospheric  
108 reanalysis dataset (ERA-Interim) and the National Aeronautic and Space Administration

109 (NASA) Modern Era Retrospective-analysis for Research and Application (MERRA)  
110 reanalysis data (Lucchesi, 2012). Moreover, there are also several global or regional  
111 LSM-based runoff simulations from GLDAS and the Variable Infiltration Capacity  
112 (VIC) model (Zhang et al., 2014). A few attempts have been made to validate multiple  
113 datasets for certain water budget components and to explore their possible  
114 hydrological implications, for example, Li X. et al. (2014) and Liu W. et al. (2016a)  
115 evaluated multiple ET estimates against the water balance method at annual and  
116 monthly time scales. Bai et al. (2016) assessed streamflow simulations of GLDAS  
117 LSMs in five major rivers over the TP based on the discharge observations. Although  
118 there are certain uncertainties among different datasets with various spatial and  
119 temporal resolutions and calculated through different algorithms (Xia et al., 2012),  
120 they do provide a great chance for us to quantify the general basin-wide water budgets  
121 and their uncertainties in gauge-sparse regions such as the TP considered in this study.  
122

123 The objectives of this study are (1) to investigate the general water budgets in 18 river  
124 basins across the Tibetan Plateau from the perspective of multiple datasets, and (2) to  
125 evaluate the seasonal cycles and annual trends of water budget components for 18 TP  
126 basins. The paper is organized as follows: the datasets and methods applied in this  
127 study are described in Sect.2. The results of season cycles and annual trends of water  
128 budget components for 18 TP basins are presented and discussed in Sect.3. The  
129 uncertainties inherited from multiple datasets are also discussed. In the Sect.4, we  
130 summarized the general results which would be helpful for understanding the water  
131 balances of the TP Rivers located at westerlies-dominated, Indian  
132 monsoon-dominated and East Asian monsoon-dominated regions.

133

## 134 **2 Data and Method**

### 135 **2.1 Multiple datasets used**

#### 136 **2.1.1 Study basins**

137 Eighteen river basins over the TP (Fig.1) with the drainage area ranging from 2832 to  
138 191235 km<sup>2</sup> (Table 1) are chosen in this study due to the availability of runoff data  
139 during the period 1982-2011. They mainly locate at the northwestern, southeastern  
140 and eastern parts of the plateau with multiyear-mean and basin-averaged temperature  
141 and precipitation ranging from -5.68 to 0.97 °C and 128 to 717 mm, which are solely  
142 or combined controlled by the westerlies, the Indian Summer monsoon and the Easter  
143 Asian monsoon (Yao et al., 2012). The glacier and snow covers are relatively more for  
144 the westerlies-dominant basins such as Yerqiang, Yulongkashi and Keliya  
145 (10.86~23.27% and 29.16~35.95%, respectively) whereas are less for the East Asian  
146 monsoon-dominated basins such as Yellow, Yangtze and Bayin (0~0.96% and  
147 9.42~20.05%, respectively) (Table 1).

148 [<Figure 1, here please, thanks>](#)

149 [<Table 1, here please, thanks>](#)

#### 150 **2.1.2 Runoff, Precipitation and Terrestrial storage change**

151 Observed daily runoff (Q) during the period 1982-2011 was obtained from the  
152 National Hydrology Almanac of China (Table 2). There are < 30% missing data in  
153 some gauging stations such as Yajiang, Tongren, Gandatan and Zelingou. Therefore,  
154 the VIC Retrospective Land Surface Dataset over China (1952~2012, VIC\_IGSNRR  
155 simulated) with a spatial resolution of 0.25 degree and a daily temporal resolution  
156 from the Geographic Sciences and Natural Resources Research (IGSNRR), Chinese  
157 Academy of Sciences, is also used. This dataset is derived from the VIC model forced  
158 by the gridded daily observed forcing (IGSNRR\_forcing) (Zhang et al., 2014). A

159 degree-day scheme was used in the model to consider the influences of snow and  
160 glacier on hydrological processes.

161

162 Monthly gridded precipitation dataset (0.5 degree, 1961-2011) from CMA, which was  
163 interpolated from observations of 2472 national meteorological stations using the  
164 Thin Plate Spline method, was used in this study (Table 2). Considering the  
165 uncertainty of CMA precipitation over the TP due to the relatively sparse stations and  
166 the complex terrain conditions, two other precipitation datasets (IGSNRR\_forcing and  
167 TRMM (Tropical Rainfall Measuring Mission) 3B43 V7, Huffman et al., 2012) were  
168 also used. The precipitation from IGSNRR forcing datasets (0.25 degree) was derived  
169 by interpolating gauged daily precipitation from 756 CMA stations based on the  
170 synergraphic mapping system algorithm (Shepard, 1984; Zhang et al., 2014) and was  
171 further bias-corrected using the CMA gridded precipitation.

172 <Table 2, here please, thanks>

173 Three latest global terrestrial water storage anomaly and water storage change ( $\Delta S$ )  
174 datasets (available on the GRACE Tellus website: <http://grace.jpl.nasa.gov/>) retrieved  
175 from the Gravity Recovery and Climate Experiment (GRACE, Tapley et al., 2004;  
176 Landerer and Swenson, 2012; Long et al., 2014), which were processed separately at  
177 the Jet Propulsion Laboratory (JPL), the GeoForschungsZentrum (GFZ) and the  
178 Center for Space Research at the University of Texas (CSR), were used. The GRACE  
179 retrievals (2002-2013) from three processing centers were averaged and a glacier  
180 isostatic adjustment correction as well a destriping filter were applied to minimize the  
181 errors and uncertainties of extracted  $\Delta S$ .

182

### 183 **2.1.3 Temperature, potential evaporation and ET**



184 The CMA monthly gridded temperature (0.5 degree) and potential evaporation (PET)  
185 dataset (0.5 degree, Harris et al., 2013) from Climatic Research Unit (CRU) in the  
186 University of East Anglia were used in this study. Moreover, six published  
187 global/regional ET products (four diagnostic products and two LSMs simulations,  
188 Table 2), namely (1) GLEAM\_E (Miralles et al., 2010, 2011), which estimated three  
189 sources of ET (transpiration, soil evaporation and interception) separately through  
190 bare soil, short vegetation and vegetation with a tall canopy through a set of algorithm  
191 ([www.gleam.eu](http://www.gleam.eu)), (2) GNoah\_E simulated by GLDAS-2 with the Catchment Noah  
192 scheme (<http://disc.sci.gsfc.nasa.gov/hydrology/data-holdings>) (Rodell et al., 2004),  
193 (3) Zhang\_E (Zhang et al., 2010) estimated using the modified Penman-Monteith  
194 approach forced with MODIS data, satellite-based vegetation parameters and  
195 meteorological observations (<http://www.nts.gov.au/project/et>), (4) MET\_E (Jung  
196 et al., 2010) (<https://www.bgc-jena.mpg.de/geodb/projects/Home.phs>), (5) VIC\_E  
197 (Zhang et al., 2014) from VIC\_IGSNRR simulations  
198 ([http://hydro.igsnrr.ac.cn/public/vic\\_outputs.html](http://hydro.igsnrr.ac.cn/public/vic_outputs.html)) and (6) PML\_E (Zhang Y. et al.,  
199 2016) computed from global observation-driven Penman-Monteith-Leuning (PML)  
200 model (<https://data.csiro.au/dap/landingpage?pid=csiro:17375&v=2&d=true>).

201

#### 202 **2.1.4 Vegetation and snow/glacier parameters**

203 The Normalized Difference Vegetation Index (NDVI) and the Leaf Area Index (LAI)  
204 were used to quantify the dynamics of vegetation for 18 TP basins (Table 2). The  
205 NDVI data was obtained from the Global Inventory Modeling and Mapping Studies  
206 (GIMMS) (Turker et al., 2005)

207 ([https://nex.nasa.gov/nex/projects/1349/wiki/general\\_data\\_description\\_and\\_access/](https://nex.nasa.gov/nex/projects/1349/wiki/general_data_description_and_access/))  
208 while the LAI data was collected from the Global Land Surface Satellite (GLASS)  
209 products (<http://www.glcf.umd.edu/data/lai/>) (Liang and Xiao, 2012). Seasonal snow  
210 and glacier are widespread over the plateau which significantly influences the water  
211 and energy budgets in the TP, but their observations are difficult due to the harsh  
212 environment, especially at the basin scale. However, there are currently a few  
213 satellite-based or LSM-simulated products which could provide general information  
214 about the variations of snow and glacier. The daily cloud free snow composite product  
215 from MODIS Terra-Aqua and the Interactive Multisensor Snow and Ice Mapping  
216 System for the Tibetan Plateau was applied to quantify the snow cover changes for  
217 each basin (Zhang et al., 2012; Yu et al., 2015). The snow water equivalent (SWE)  
218 retrieved from Global Snow Monitoring for Climate Research product (GlobSnow-2,  
219 <http://www.globsnow.info/>) and the VIC\_IGSNRR simulations were also used in this  
220 study (Takala et al., 2011; Zhang et al., 2014). Moreover, the Second Glacier  
221 Inventory Dataset of China was used to extract the general distribution of glacier  
222 (Guo et al., 2014). All gridded datasets used were first uniformly interpolated to a  
223 spatial resolution of 0.5 degree based on the bilinear interpolation to make their  
224 inter-comparison possible. The datasets were then extracted for each of TP basins.

225

### 226 **2.1.5 Monsoon indices**

227 The TP climate is generally influenced by the westerlies, Indian summer monsoon and  
228 East Asian summer monsoon (Yao et al., 2012). To investigate the changes of  
229 monsoon systems and their potential influences on the water budget in the TP basins,  
230 three monsoon indices, namely Asian Zonal Circulation Index (AZCI), Indian Ocean  
231 Dipole Mode Index (IODMI) and East Asian Summer Monsoon Index (EASMI), are

232 used in this study. The IODMI is an indicator of the east-west temperature gradient  
233 across the tropical Indian Ocean defined by Saji et al. (1999), which can be  
234 downloaded from the following website:  
235 [http://www.jamstec.go.jp/frcgc/research/d1/iod/HTML/Dipole%20Mode%20Index.ht](http://www.jamstec.go.jp/frcgc/research/d1/iod/HTML/Dipole%20Mode%20Index.html)  
236 [ml](http://www.jamstec.go.jp/frcgc/research/d1/iod/HTML/Dipole%20Mode%20Index.html). The EASMI and AZCI (60°-150°E) reflect the dynamics of East Asian summer  
237 monsoon (Li and Zeng, 2002) and the westerlies, which can be obtained from the  
238 <http://ljp.gcess.cn/dct/page/65577> and the National Climate Center of China  
239 (<http://ncc.cma.gov.cn/Website/index.php?ChannelID=43WCHID=5>), respectively.

## 240 **2.2 Methods**

### 241 **2.2.1 Water balance-based ET estimation**

242 The basin-wide water balance at the monthly and annual timescales could be written  
243 as the principle of mass conservation (also known as the continuity equation,  
244 Oliverira et al., 2014) of basin-wide precipitation ( $P$ , mm), evapotranspiration ( $ET_{wb}$ ,  
245 mm), runoff ( $Q$ , mm) as well as terrestrial water storage change ( $\Delta S$ , mm),

$$246 \quad ET_{wb} = P - Q - \Delta S \quad (1)$$

247 In most TP basins, glacier melt ( $M_G$ , mm) contributes to river discharge together with  
248 precipitation (liquid precipitation and snow). The monthly and annual water balance  
249 in these basins can thus be revised as,

$$250 \quad ET_{wb} = P + M_G - Q - \Delta S \quad (2)$$

251 Several attempts have been made for separating glacier contributions to river  
252 discharge through site-scale isotopic observations, remote sensing as well as  
253 land-surface hydrological modeling for some individual TP basins (Zhang et al., 2013;  
254 Zhou et al., 2014; Neckel et al., 2014; Xiang et al., 2016). However, accurate  
255 quantification of  $M_G$  is difficult in the data-sparse TP, especially for multiple basins.  
256 In this study, we simply use the percentages of glacier melt to river discharge for

257 some TP basins derived from the literatures (Chen, 1988; Mansur and Ajnis, 2005;  
258 Zhang et al., 2013; Liu J. et al., 2016) and the empirical relations between the glacier  
259 area ratio (%) and glacier melt in basins mentioned above (Table 3).

260 <Table 3, here please, thanks>

261 The terrestrial water storage ( $\Delta S$ ) in Eq.(2), which includes the surface, subsurface  
262 and ground water changes, cannot be neglected in water balance calculation at a  
263 monthly or annual timescale due to snow accumulation and some anthropogenic  
264 interferences such as reservoir regulation and agriculture irrigation (Liu W. et al.,  
265 2016a). The water balance-based ET ( $ET_{wb}$ ) during 2002-2011 can be calculated  
266 through Eq. (2) using the GRACE-derived mass anomaly as  $\Delta S$ . For  $ET_{wb}$   
267 calculation before 2002 when the GRACE data is unavailable, we use a two-step bias  
268 correction procedure (Li X. et al., 2014) to close the water balance at monthly  
269 timescale considering the  $\Delta S$ . We define  $P + M_G - Q$  as biased ET ( $ET_{biased}$ ,  
270 available from 1982-2011) relative to the  $ET_{wb}$  (available from 2002-2011 when the  
271 GRACE data is available) calculated from Eq. (2). Firstly, the  $ET_{biased}$  and  $ET_{wb}$   
272 series over the period 2002-2011 were separately fitted using a gamma distribution,  
273 which has been evidenced as an proper method for modeling the probability  
274 distribution of ET (Bouraoui et al., 1999). The value in monthly  $ET_{biased}$  series  
275 (2002-2011) can be bias-corrected through the inverse function ( $F^{-1}$ ) of the gamma  
276 cumulative distribution function (CDF,  $F$ ) of  $ET_{wb}$  by matching the cumulative  
277 probabilities between two CDFs as follow (Liu W. et al., 2016a),

$$ET_{wb}(m) = F^{-1}(F(ET_{biased}(m)|\alpha_{biased}, \beta_{biased})|\alpha_{wb}, \beta_{wb}) \quad (3)$$

279 Here  $\alpha_{biased}$ ,  $\beta_{biased}$ ,  $\alpha_{wb}$  and  $\beta_{wb}$  are the shape and scale parameters of gamma  
280 distribution for  $ET_{biased}$  and  $ET_{wb}$ . The second step is to eliminate the annual bias  
281 through the ratio of annual  $ET_{biased}$  to annual  $ET_{wb}$  calculated in the first step using

282 the following method,

$$283 \quad ET_{wb}(m) = \frac{ET_{biased(a)}}{ET_{wb(a)}} \times ET_{wb}(m) \quad (4)$$

284 The procedure was then applied to correct the monthly  $ET_{biased}$  series and calculated  
285 the monthly  $ET_{wb}$  during the period 1982-2001 for all TP basins. The  $ET_{wb}$  obtained  
286 was seemed as the “true” ET for evaluating multiple ET products and further for the  
287 trend analysis.

### 288 **2.2.2 Modified Mann-Kendall test method**

289 The Mann-Kendall (MK) test is a rank-based nonparametric approach which is less  
290 sensitive to outlier relative to other parametric statistics, but it is sometimes  
291 influenced by the serial correlation of time series. Pre-whitening is often used to  
292 eliminate the influence of lag-1 autocorrelation before the use of MK test, for example,  
293 in pre-whitening, the analyzed time series  $(X_1, X_2, \dots, X_n)$  will be replaced by  
294  $(X_2 - cX_1, X_3 - cX_2, \dots, X_{n+1} - cX_n)$  if the lag-1 autocorrelation coefficient ( $c$ ) is  
295 larger than 0.1 (von Storch, 1995). However, significant lag- $i$  autocorrelation may still  
296 be detected after pre-whitening because only the lag-1 autocorrelation is considered in  
297 pre-whitening (Zhang et al., 2013). Moreover, it sometimes underestimate the trend  
298 for a given time series (Yue et al., 2002). Hamed and Rao (1998) proposed a modified  
299 version of MK test (MMK) to consider the lag- $i$  autocorrelation and related robustness  
300 of the autocorrelation through the use of equivalent sample size, which has been  
301 widely used in previous studies during the last five decades (McVicar et al., 2012;  
302 Zhang et al., 2013; Liu and Sun, 2016). In the MMK approach, if the lag- $i$   
303 autocorrelation coefficients are significantly distinct from zero, the original variance  
304 of MK statistics will be replaced by the modified one. In this study, we used the  
305 MMK approach to quantify the trends of water budget components in 18 TP basins  
306 and the significance of trend was tested at the >95% confidence level.

### 307 **3 Results and Discussion**

#### 308 **3.1 ET evaluation and General hydrological characteristics of 18 TP basins**

309 In this study, we first assess the VIC\_IGSNRR simulated runoff against the  
310 observations for each basin (for example, at Tangnaihai and Pangduo stations in  
311 Fig.2). The VIC\_IGSNRR simulated runoff is acceptable and could be used to replace  
312 the missing values for a given basin, if the Nash Efficiency coefficient (NSE) between  
313 the observation and simulation is above 0.65. Moreover, the CMA precipitation is  
314 consistent with TRMM (Corr = 0.86, RMSE = 8.34 mm/month) and IGSNRR forcing  
315 (Corr = 0.94, RMSE = 7.15mm/month) precipitation for multiple basins (and also for  
316 the smallest basin above Tongren station, Fig.2), which reveals the applicability of CMA  
317 precipitation under the TP conditions.

318 [< Figure 2, here please, thanks >](#)

319 We then evaluated six ET products in 18 TP basins against our calculated  $ET_{wb}$  at a  
320 monthly basis (Fig. 3). The ranges of monthly averaged ET among different basins  
321 (approximately 4–39 mm month<sup>-1</sup>) are very close for all products compared with that  
322 calculated from the  $ET_{wb}$  (6–42 mm month<sup>-1</sup>). However, GLEAM\_E (correlation  
323 coefficient: Corr = 0.85 and root-mean-square-error: RMSE = 5.69 mm month<sup>-1</sup>) and  
324 VIC\_E (Corr = 0.82 and RMSE = 6.16 mm month<sup>-1</sup>) perform relatively better than  
325 others. Although Zhang\_E and GNoah\_E were found closely correlated to  
326 monthly  $ET_{wb}$  in the upper Yellow River, the upper Yangtze River, Qiangtang and  
327 Qaidam basins (Li X. et al., 2014), they did not exhibit overall good performances  
328 (Corr = 0.61, RMSE = 7.97 mm month<sup>-1</sup> for Zhang\_E and Corr = 0.42, RMSE =  
329 10.16 mm month<sup>-1</sup> for GNoah\_E) for 18 TP basins used in this study. We thus use  
330 GLEAM\_E and VIC\_E together with  $ET_{wb}$  to calculate the seasonal cycles and  
331 trends of ET in 18 TP basins in the following sections.

332 < Figure 3, here please, thanks >

333 To investigate the general hydroclimatic characteristics of rivers over the TP, we  
334 classify 18 basins into three categories, namely westerlies-dominated basins  
335 (Yerqiang, Yulongkashi and Kelia), Indian monsoon-dominated basins (Brahmaputra  
336 and Salween), and East Asian monsoon-dominated basins (Yellow, Yalong and  
337 Yangtze) referred to Tian et al. (2007), Yao et al. (2012) and Dong et al. (2016).  
338 Interestingly, they are clustered into three groups under Budyko framework (Budyko,  
339 1974; Zhang D. et al., 2016) with relatively lower evaporative index for Indian  
340 monsoon-dominant basins and higher aridity index for westerlies-dominant basins,  
341 which reveal various long-term hydroclimatologic conditions (Fig. 4). Overall, the  
342 annual mean air temperature increases (-5.68 ~0.97 °C) while multiyear mean glacier  
343 area (and thus the glacier melt normalized by precipitation) decreases (23.27 ~ 0%)  
344 gradually from the westerlies-dominant, Indian monsoon-dominant to East Asian  
345 monsoon-dominant basins. The vegetation status (NDVI range: 0.05~0.43; LAI range:  
346 0.03~0.83) tends to be better and ET increases (and thus runoff coefficient gradually  
347 decreases) from cold to warm basins (Fig. 4 and Table 1). The  $R^2$  between  
348 basin-averaged NDVI and ET is 0.76 which shows a clear vegetation control on ET in  
349 18 TP basins. The result is in line with Shen et al. (2015), which indicated that the  
350 spatial pattern of ET trend was significantly and positively correlated with NDVI  
351 trend over the TP. It is a general picture of hydrological regime in high-altitude and  
352 cold regions (Zhang et al., 2013; Cuo et al., 2014), which could be interpreted from  
353 the perspective of multi-source datasets in the data-sparse TP.

354 < Figure 4, here please, thanks >

### 355 **3.2 Seasonal cycles of basin-wide water budget components for the TP basins**

356 The multi-year means of water budget components (i.e., P, Q, ET, snow cover and

357 SWE) and vegetation parameters (i.e., NDVI and LAI) were calculated for each  
358 calendar month and for 18 TP river basins using multi-source datasets available from  
359 1982 to 2011. Overall, the seasonal variations of P, Q, ET, air temperature and  
360 vegetation parameters are similar in all TP basins with peak values occurred in May to  
361 September (Fig.5 and Fig.6). The seasonal cycles of snow cover and SWE are  
362 generally time consistent as well for 18 TP basins (the peak values mainly occur from  
363 October to next April, Fig.7). With the ascending air temperature from cold to warm  
364 months, the basin-wide precipitation increases and vegetation turns green gradually  
365 (the basin-wide ET also increase). Meanwhile, glacier and snow melt or vanish  
366 gradually with the melt water supply the river discharge together with precipitation.  
367 The inter-basin variations of hydrological regime are to a large extent linked to the  
368 climate systems that prevail over the TP.

369 [< Figure 5, here please, thanks >](#)

370 Although the temporal patterns of hydrological components are general analogous,  
371 they varied among parameters, climate zones and even basins (Zhou et al., 2005). For  
372 example, relative to air temperature, the seasonal variation of runoff is more similar to  
373 precipitation which reveals that runoff is mainly controlled by precipitation in most  
374 TP basins. It is in agreement with that summarized by Cuo et al. (2014). In the  
375 westerlies-dominated basins, the peak values of precipitation and runoff mainly  
376 concentrate in June-August, which contribute approximately 68-82% and 67-78% of  
377 annual totals, respectively. During this period, the runoff always exceeds precipitation  
378 which indicates large contributions of glacier/snow-melt water to streamflow. It is  
379 consistent with the existing findings in Tarim River (Yerqiang, Yulongkashi and  
380 Keliya rivers are the major tributaries of Tarim River), which indicated that the melt  
381 water accounted for about half of the annual total streamflow (Fu et al., 2008). The



382 ET (vegetation cover) in three westerlies-dominated basins are relatively less (scarcer)  
383 than that in other TP basins while the percentages of glacier and seasonal snow cover  
384 are higher in these basins which contribute more melt water to river discharge (Fig.6  
385 and Fig.7). Overall, the SWE in Yerqiang, Yulongkashi and Keliya rivers are  
386 relatively higher in winter than other seasons, but they vary with basins and products  
387 which reveal considerable uncertainties in SWE estimations.

388 [< Figure 6, here please, thanks >](#)

389 In the Indian monsoon and East Asian monsoon-dominated basins, the runoff  
390 concentrates during June-September (or June- October) with precipitation being the  
391 dominant contributor of annual total runoff. For example, the peak values of  
392 precipitation and runoff occur during June-September at Zhimenda station  
393 (contributing about 80% and 74% of the annual totals) while those occur during  
394 June-October at Tangnaihahai station (contributing about 78% and 71% of the annual  
395 totals, respectively). The results are quite similar to the related studies in eastern and  
396 southern TP such as Liu (1999), Dong et al. (2007), Zhu et al. (2011), Zhang et al.  
397 (2013), Cuo et al. (2014). The vegetation cover (ET) in most basins is relatively better  
398 (higher) than that in the westerlies-dominant basins. Moreover, the seasonal snow  
399 mainly covers from mid-autumn to spring and correspondingly the SWE is relatively  
400 higher in these months in all basins except for Yellow River above Xining station,  
401 Salwee River above Jiayuqiao station and Brahmaputra River above Nuxia and  
402 Yangcun stations.

403 [< Figure 7, here please, thanks >](#)

### 404 **3.3 Trends of basin-wide water budget components for the TP basins**

405 Trends in water budget components for 18 TP basins during the period 1982-2011  
406 were also examined through the modified Mann-Kendall test (MMK) in this study.

407 The hydrological cycles intensified in the westerlies-dominated basins with Q, P and  
408  $ET_{wb}$  all ascended with regional warming (Fig.8), especially in the Keliya River  
409 basin (Numaitilangan station). The aridity index (PET/P), which is an indicator for the  
410 degree of dryness, slightly declined in all basins in northwestern TP. Although P and  
411 PET were found both increase since the 1980s (Shi et al., 2003; Yao et al., 2014), the  
412 declined PET/P is, to some extent, attributed to the ascending P exceed the increase in  
413 PET for these basins (except for the Yulongkashi basin). The climate moistening in  
414 the headwaters of these inland rivers would be beneficial to the water resources and  
415 oasis agro-ecosystems in the middle and lower basins. The increase in streamflow was  
416 also found in most tributaries of the Tarim River (Sun et al., 2006; Fu et al., 2010;  
417 Mamat et al., 2010). Moreover, the westerlies, revealed by the Asian Zonal  
418 Circulation Index ( $60^{\circ}$ - $150^{\circ}$  E), slightly enhanced (linear trend: 0.21) over the period  
419 of 1982-2011 (Fig.9). More water vapor was transported and fell as precipitation or  
420 snow in northwestern TP (e.g., the eastern Pamir region) with the strengthening  
421 westerlies. Both SWE products (VIC\_IGSNRR simulated and GlobaSnow-2 product)  
422 showed slightly increase for all basins with the incremental seasonal snow cover and  
423 advanced glaciers (Yao et al., 2012). More precipitation was transformed into snow or  
424 glacier and the runoff coefficient (Q/P) exhibited decrease although precipitation  
425 obviously increased (Fig.8). In addition, the transpiration in these basins may decrease  
426 with vegetation degradation revealed by the NDVI and LAI (Yin et al., 2016) but the  
427 atmospheric evaporative demand indicated by CRU PET increased (significantly  
428 increase in the Yulongkashi and Keliya rivers) during the period 1982-2011.

429 [< Figure 8, here please, thanks >](#)

430 [< Figure 9, here please, thanks >](#)

431 In the East Asian monsoon-dominated basins, there are two types of change for

432 basin-wide water budget components. For example, P and Q slightly decreased in the  
433 upper Yellow River (Tangnihai, Huangheyan and Jimai stations) and Yalong River  
434 (Yajiang station) but increased in other basins (Zelingou, Gandatan, Xining, Tongren  
435 and Zhimenda stations) over the period of 1982-2011 (Fig.10). The decline in Q and P  
436 for the upper Yellow and Yalong Rivers (locate at the eastern Tibetan Plateau) were  
437 consistent with that found by Cuo et al. (2013, 2014) as well as Yang et al. (2014), and  
438 were in line with the weakening (linear slope: -0.01) of the East Asian Summer  
439 Monsoon (Fig.9). The vegetation turned green while  $ET_{wb}$  and PET increased in all  
440 nine basins with the significantly ascending air temperature during the period  
441 1982-2011. The aridity index (PET/P) was found decrease in all basins except for the  
442 upper Yellow River basin above Jimai station and the upper Yalong River basin above  
443 Yajiang station. Moreover, both the runoff coefficients and SWE were decrease except  
444 for the Bayin River above Zelingou station and the upper Yellow River above Tongren  
445 station in the East Asian monsoon dominated basins.

446 < Figure 10, here please, thanks >

447 The hydrological cycles were also found intensified in the Indian monsoon-dominated  
448 basins such as Salween River and Brahmaputra River (Fig.11), which were in line  
449 with the strengthen (linear trend: 0.01) of the Indian Summer monsoon (revealed by  
450 the Indian Ocean Dipole Mode Index) during the specific period 1982-2011 (Fig.9).  
451 In the six basins, trends in P, Q and  $ET_{wb}$  were all upward. For example, at  
452 Jiayuqiao station, the annual streamflow showed slightly increasing trend which was  
453 consistent with that examined during 1980-2000 by Yao et al. (2012). The vegetation  
454 status, revealed by NDVI and LAI, turned better significantly with the ascending air  
455 temperature. The aridity index (PET/P) decreased in all basins except for the  
456 Brahmaputra River above Tangjia station, which indicated that most basins in the

457 Indian monsoon-dominated regions turn wet over the period of 1982-2011. The runoff  
458 coefficient (Q/P) increased at Gongbujiangda and Nuxia while decreased at Jiayuqiao,  
459 Pangduo, Tangji and Yangcun stations. Moreover, the basin-wide SWE declined in the  
460 upper Salween River and Brahmaputra River above Pangduo, Tangjia and  
461 Gongbujiangda stations while increased in Brahmaputra River above Nuxia and  
462 Yangcun stations.

463 [< Figure 11, here please, thanks >](#)

#### 464 **3.4 Uncertainties**

465 The results may unavoidably associate with several aspects of uncertainties which  
466 mainly inherited from the multi-source datasets used. For example, although the  
467 seasonal cycles of  $ET_{wb}$  can be captured by GLEAM\_E and VIC\_E, they still have  
468 considerable uncertainties such as at Numaitilangan, Gongbujiangda and Nuxia  
469 stations (Fig.5). With respect to the annual trend of  $ET_{wb}$  (Table 4), most ET products  
470 (including the well-performed GLEAM\_E and VIC\_E in some basins) cannot detect  
471 the decreasing trends in 7 out of 18 basins (at Kulukelangan, Tongguziluoke, Xining,  
472 Tongren, Jimai, Nuxia and Gongbujiangda stations). We thus only used  $ET_{wb}$  in the  
473 trend detection of water budget components in Fig.8, Fig.10 and Fig.11 in this study.  
474 The two SWE products also showed large uncertainty, with respect to both their  
475 seasonal cycles and trends due to their different forcing data; different algorithms  
476 applied as well as varied spatial-temporal resolutions. Moreover, the interpolation of  
477 missing values of runoff with VIC\_IGSNRR simulated runoff and the gridded  
478 precipitation data (which interpolated from limited gauged precipitation over the  
479 plateau) involved some uncertainties as well as. Finally, we obtained the contributions  
480 of glacier-melt to discharge in some basins from the literatures and took them as fixed  
481 numbers. It may inherit considerable uncertainty from varied studies using different

482 approaches such as glacier mass-balance observation, isotope observation and  
483 hydrological modeling, and the contribution rates would also change under a warming  
484 climate. However, accurate quantification of the contribution of glacier-melt to  
485 discharge is technically difficult nowadays, especially for the data-sparse basins. With  
486 these caveats, we can interpret the general hydrological regimes and their responses to  
487 the changing climate in the TP basins from solely the perspective of multi-source  
488 datasets, which are comparable to the existing studies based on the in situ  
489 observations and complex hydrological modeling.

490 [<Table 4, here please, thanks>](#)

#### 491 **4 Summary**

492 In this study, we investigated the seasonal cycles and trends of water budget  
493 components in 18 TP basins during the period 1982-2011, which is not well  
494 understood so far due to the lack of adequate observations in the harsh environment,  
495 through integrating the multi-source global/regional datasets such as gauge data,  
496 satellite remote sensing and land surface model simulations. By using a two-step bias  
497 correction procedure, annual basin-wide  $ET_{wb}$  was calculated through the water  
498 balance considering the impacts of glacier and water storage change. The GLEAM\_E  
499 and VIC\_E were found perform better relative to other products against the  
500 calculated  $ET_{wb}$ .

501

502 The general water and energy budgets were different in the westerlies-dominated  
503 (with higher aridity index, runoff coefficient and glacier cover), the Indian  
504 monsoon-dominated and the East Asian monsoon-dominated (with higher air  
505 temperature, vegetation cover and evapotranspiration) basins under the perspective of  
506 Budyko framework. In 18 TP basins, precipitation is the major contributor to the river

507 runoff, which concentrates mainly during June-October (June-August for the  
508 westerlies-dominated basins, June-September or June to October for the Indian  
509 monsoon-dominated and the East Asian monsoon-dominated basins). The basin-wide  
510 SWE is relatively higher from mid-autumn to spring for all 18 TP basins except for  
511 Keliya River and Brahmaputra River above the Nuxia and Yangcun stations. The  
512 vegetation cover is relatively less whereas snow/glacier cover is more in the  
513 westerlies-dominant basins compared with other basins. The hydrological cycles were  
514 found intensified under the regional warming in most TP basins except for most  
515 tributaries of the upper Yellow River and the Yalong River, which were significantly  
516 influenced by the weakening East Asian monsoon during the period 1982-2011. The  
517 aridity index (PET/P) exhibited decrease in most TP basins which corresponded to the  
518 warming and moistening climate in the TP and western China. Moreover, the runoff  
519 coefficient (Q/P) declined in most basins which may be, to some extent, due to ET  
520 increase induced by vegetation greening and the influences of snow and glacier  
521 changes. Although there are considerable uncertainties inherited from multi-source  
522 data used, the general hydrological regimes in the TP basins could be revealed, which  
523 are consistent to the existing results obtained from in situ observations and complex  
524 land surface modeling. It indicated the usefulness of integrating the multiple datasets  
525 available such as in situ observations, remote sensing-based products, reanalysis  
526 outputs, land surface model simulations and climate model outputs for hydrological  
527 applications. The results obtained could be helpful for understanding the hydrological  
528 cycles and further for the water resources management and eco-environment  
529 protection under a warming climate in the vulnerable Tibetan Plateau.

530

531 ***Author contributions.*** Wenbin Liu and Fubao Sun developed the idea to see the

532 general water budgets in the TP basins from the perspective of multisource datasets.  
533 Wenbin Liu collected and processed the multiple datasets with the help of Yanzhong  
534 Li, Guoqing Zhang, Hong Wang as well as Peng Bai, and prepared the manuscript.  
535 The results were extensively commented and discussed by Fubao Sun, Jiahong Liu  
536 and Yan-Fang Sang.

537

538 **Acknowledgements.** This study was supported by the National Key Research and  
539 Development Program of China (2016YFC0401401 and 2016YFA0602402), National  
540 Natural Science Foundation of China (41401037 and 41330529), the Open Research  
541 Fund of State Key Laboratory of Desert and Oasis Ecology in Xinjiang Institute of  
542 Ecology and Geography, Chinese Academy of Sciences (CAS), the CAS Pioneer  
543 Hundred Talents Program (Fubao Sun), the Initial Founding of Scientific Research  
544 (Y5V50019YE) and the program for the “Bingwei” Excellent Talents from the  
545 Institute of Geographic Sciences and Natural Resources Research, CAS. We are  
546 grateful to the NASA MEaSURES Program (Sean Swenson) for providing the  
547 GRACE land data processing algorithm. The basin-wide water budget series in the TP  
548 Rivers used in this study are available from the authors upon request  
549 ([liuwb@igsnr.ac.cn](mailto:liuwb@igsnr.ac.cn)). We wish to thank the editors and reviewers for their invaluable  
550 comments and constructive suggestions to improve the quality of the manuscript.

551

## 552 **References**

553 Akhtar, M., Ahmad, N., and Booij, M.J.: Use of regional climate model simulations as input for  
554 hydrological models for the Hindukush-Karakorum-Himalaya region, *Hydrol. Earth Syst. Sci.*  
555 13, 1075-1089, 2009.

556 Bai, P., Liu, X.M., Yang, T.T., Liang, K., and Liu, C.M.: Evaluation of streamflow simulation  
557 results of land surface models in GLDAS on the Tibetan Plateau, *J. Geophys. Res. Atmos.*, 121,

558 12180-12197, 2016.

559 Berrisford, P, Lee, D., Poli, P., Brugge, R., Fielding, K., Fuentes, M., Kallberg, P., Kobayashi, S.,  
560 Uppala, S., and Simmons, A.: The ERA-interim archive. ERA Reports Series No. 1 Version 2.0,  
561 Available from: <[https://www.researchgate.net/publication/41571692\\_The\\_ERA-interim](https://www.researchgate.net/publication/41571692_The_ERA-interim_archive)  
562 archive>, 2011.

563 Bookhagen, B. and Burbank, D.W.: Toward a complete Himalayan hydrological budget:  
564 spatiotemporal distribution of snowmelt and rainfall and their impact on river discharge, *J.*  
565 *Geophys. Res.*, 115, F03019, 2010.

566 Bouraoui, F., Vachaud, G., Li, L.Z.X., LeTretut, H., and Chen, T.: Evaluation of the impact of  
567 climate changes on water storage and groundwater recharge at the watershed scale, *Clim. Dyn.*,  
568 15(2), 153-161, 1999.

569 Budyko, M.I.: *Climate and life*. Academic Press, 1974.

570 Chen, D., Xu, B., Yao, T., Guo, Z., Cui, P., Chen, F., Zhang, R., Zhang, X., Zhang, Y., Fan, J., Hou,  
571 Z., and Zhang, T.: Assessment of past, present and future environmental changes on the Tibetan  
572 Plateau, *Chinese SCI. Bull.*, 60(32), 3025-3035, 2015 (in Chinese).

573 Chen, J.: Lichenometrical studies on glacier changes during the Holocene Epoch at the sources  
574 region of Urumqi River, *Sci. China B.*, 18(1), 95-104, 1988 (in Chinese).

575 Cuo, L., Zhang, Y.X., Bohn, T.J., Zhao, L., Li, J.L., Liu, Q.M., and Zhou, B.R.: Frozen soil  
576 degradation and its effects on surface hydrology in the northern Tibetan Plateau, *J. Geophys.*  
577 *Res. Atmos.*, 120(6), 8276-8298, 2015.

578 Cuo, L., Zhang, Y.X., Gao, Y., Hao, Z., and Cairang, L.: The impacts of climate change and land  
579 cover/use transition on the hydrology in the upper Yellow River Basin, China, *J. Hydrol.*, 502,  
580 37-52, 2013.

581 Cuo, L., Zhang, Y.X., Zhu, F.X., and Liang, L.Q.: Characteristics and changes of streamflow on  
582 the Tibetan Plateau: A review, *J. Hydrol. Reg. stud.*, 2, 49-68, 2014.

583 Dong, X., Yao, Z., and Chen, C.: Runoff variation and responses to precipitation in the source  
584 regions of the Yellow River, *Resour. Sci.*, 29(3), 67-73, 2007 (in Chinese).

585 Dong, W., Lin, Y., Wright, J.S., Ming, Y., Xie, Y., Wang, B., Luo, Y., Huang, W., Huang, J., Wang,  
586 L., Tian, L., Peng, Y., and Xu, F.: Summer rainfall over the southwestern Tibetan Plateau  
587 controlled by deep convection over the Indian Subcontinent, *Nat. Commun.*, 7, 10925, 2016.



588 Duan, A.M. and Wu, G.X.: Change of cloud amount and the climate warming on the Tibetan  
589 Plateau, *Geophys. Res. Lett.*, 33, L22704, 2006.

590 Fu, L., Chen, Y., Li, W., Xu, C., and He, B.: Influence of climate change on runoff and water  
591 resources in the headwaters of the Tarim River, *Arid Land Geogr.*, 31(2), 237-242, 2008 (in  
592 Chinese).

593 Fu, L., Chen, Y., Li, W., He, B., and Xu, C.: Relation between climate change and runoff volume  
594 in the headwaters of the Tarim River during the last 50 years., *J. Desert Res.*, 30(1), 204-209,  
595 2010 (in Chinese).

596 Guo, W.Q., Liu, S.Y., Yao, X.J., Xu, J.L., Shangguan, D.H., Wu, L.Z., Zhao, J.D., Liu, Q., Jiang,  
597 Z.L., Wei, J.F., Bao, E.J., Yu, P.C., Ding, L.F., Li, G., Ge, C.M., and Wang, Y.: The Second  
598 Glacier Inventory Dataset of China, Cold and Arid Regions Science Data Center at Lanzhou,  
599 doi: 10.3972/glacier.001.2013.db, 2014.

600 Hamed, K.H. and Rao, A.R.: A modified Mann-Kendall trend test for autocorrelation data,  
601 *J.Hydrol.*, 204(1-4), 182-196, 1998.

602 Huffman, G.J., , E.F., Bolvin, D.T., Nelkin, E.J., and Adler, R.F.: last updated 2013: TRMM  
603 Version 7 3B42 and 3B43 Data Sets, NASA/GSFC, Greenbelt, MD. Data set accessed at  
604 [http://mirador.gsfc.nasa.gov/cgi-bin/mirador/](http://mirador.gsfc.nasa.gov/cgi-bin/mirador/presentNavigation.pl?tree=project&project=TRMM&dataGroup=Gridded&CGIS)  
605 [presentNavigation.pl?tree=project&project=TRMM&dataGroup=Gridded&CGIS](http://mirador.gsfc.nasa.gov/cgi-bin/mirador/presentNavigation.pl?tree=project&project=TRMM&dataGroup=Gridded&CGIS)  
606 [ESSID=5d12e2ffa38ca2aac6262202a79d882a](http://mirador.gsfc.nasa.gov/cgi-bin/mirador/presentNavigation.pl?tree=project&project=TRMM&dataGroup=Gridded&CGIS), 2012.

607 Harris, I., Jones, P.D., Osborn, T.J., and Lister, D.H.: Updated high-resolution grids of monthly  
608 climatic observations – the CRU TS3.10 Dataset, *Int. J. Climatol.*, 34 (3), 623-642, 2014.

609 Immerzeel, W.W., van Beek, L.P.H., and Bierkens, M.F.P.: Climate change will affect the Asian  
610 water towers, *Science*, 328, 1382-1385, 2010.

611 Jung, M., Reichstein, M., Ciais, P., Seneviratne, S.I., Sheffield, J., Goulden, M.L., Bonan, G.,  
612 Cescatti, A., Chen, J., de Jeu, R., Dolman, A.J., Eugster, W., Gerten, D., Gianelle, D., Gobron, N.,  
613 Heinke, J., Kimball, J., Law, B.E., Montagnani, L., Mu, Q., Mueller, B., Oleson, K., Papale, D.,  
614 Richardson, A.D., Rouspard, O., Running, S., Tomelleri, E., Viovy, N., Weber, U., Williams, C.,  
615 Wood, E., Zaehle, S., and Zhang, K.: Recent decline in the global land evapotranspiration trend

616 due to limited moisture supply, *Nature*, 467, 951-954, 2010.

617 Kobayashi, S., Ota, Y., Harada, Y., Ebita, A., Moriya, M., Onoda, H., Onogi, K., kamahori, H.,  
618 kobayashi, C., Endo, H., miyaoka, K., and Takahashi, K.: The JRA-55 Reanalysis: General  
619 specifications and basic characteristics, *J.Meteor. Soc. Japan*, 93(1), 5-58, doi:  
620 10.2151/jmsj.2015-001, 2015.

621 Landerer, F.W. and Swenson, S.C.: Accuracy of scaled GRACE terrestrial water storage estimates,  
622 *Water Resour.Res.*, 48, W04531, 2012.

623 Li, F.P., Zhang, Y.Q., Xu, Z.X., Liu, C.M., Zhou, Y.C., and Liu, W.F.: Runoff predictions in  
624 ungauged catchments in southeast Tibetan Plateau, *J. Hydrol.*, 511, 28-38, 2014.

625 Li, F.P., Zhang, Y.Q., Xu, Z.X., Teng, J., Liu, C.M., Liu, W.F., and Mpelasoka, F.: The impact of  
626 climate change on runoff in the southeastern Tibetan Plateau, *J. Hydrol.*, 505, 188-201, 2013.

627 Li, J.P. and Zeng, Q.C.: A unified monsoon index, *Geophy. Res. Lett.*, 29(8), 1274, 2002.

628 Li, X.P., Wang, L., Chen, D.L., Yang, K., and Wang, A.H.: Seasonal evapotranspiration changes  
629 (1983-2006) of four large basins on the Tibetan Plateau, *J. Geophys. Res.*, 119 (23),  
630 13079-13095, 2014.

631 Liang, S.L. and Xiao, Z.Q.: Global Land Surface Products: Leaf Area Index Product Data  
632 Collection(1985-2010), Beijing Normal University, doi:10.6050/glass863.3004.db, 2012.

633 Liu, J., Liu, T., Bao, A., De Maeyer, P., Feng, X., Miller, S.N., and Chen, X.: Assessment of  
634 different modeling studies on the spatial hydrological processes in an arid alpine catchment,  
635 *Water Resour. Manag.*, 30, 1757-1770, 2016.

636 Liu, T.: Hydrological characteristics of Yalungzangbo River, *Acta Geogr. Sin.*, 54 (Suppl.),  
637 157-164, 1999 (in Chinese).

638 Liu, W.B. and Sun, F.B.: Assessing estimates of evaporative demand in climate models using  
639 observed pan evaporation over China, *J. Geophys. Res. Atmos.*, 121, 8329-8349, 2016.

640 Liu, W.B., Wang, L., Zhou, J., Li, Y.Z., Sun, F.B., Fu, G.B., Li, X.P., and Sang, Y-F.: A worldwide  
641 evaluation of basin-scale evapotranspiration estimates against the water balance method, *J.*  
642 *Hydrol.*, 538, 82-95, 2016a.

643 Liu, W.B., Wang, L., Chen, D.L., Tu, K., Ruan, C.Q., and Hu, Z.Y.: Large-scale circulation  
644 classification and its links to observed precipitation in the eastern and central Tibetan Plateau,  
645 *Clim. Dyn.*, 46, 3481-3497, 2016b.

646 Liu, X.M., Yang, T., Hsu, K., Liu, C., and Sorooshian, S.: Evaluating the streamflow simulation  
647 capability of PERSIANN-CDR daily rainfall products in two river basins on the Tibetan Plateau,  
648 *Hydrol. Earth Syst. Sci. Discuss.*, doi: 10.5194/hess-20160282, 2016.

649 Long, D., shen, Y.J., Sun, A., Hong, Y., Longuevergne, L., Yang, Y.T., Li, B., and Chen, L.:  
650 Drought and flood monitoring for a large karst plateau in Southwest China using extended  
651 GRACE data, *Remote Sen. Environ.*, 155, 145-160, 2014.

652 Lucchesi, R.: File specification for MERRA products, GMAO Office Note No.1 (version 2.3), 82  
653 pp, available from [http://gmao.gsfc.nasa.gov/pubs/office\\_notes](http://gmao.gsfc.nasa.gov/pubs/office_notes), 2012.

654 Ma, N., Szilagyi, J., Niu, G.Y., Zhang, Y.S., Zhang, T., Wang, B.B., and Wu, Y.H.: Evaporation  
655 variability of Nam Co Lake in the Tibetan Plateau and its role in recent rapid lake expansion, *J.*  
656 *Hydrol.*, 537, 27-35, 2016.

657 Ma, N., Zhang, Y.S., Guo, Y.H., Gao, H.F., Zhang, H.B., and Wang, Y.F.: Environmental and  
658 biophysical controls on the evapotranspiration over the highest alpine steppe, *J. Hydrol.*, 529,  
659 980-992, 2015.

660 Mamat, A., Halik, W., and Yang, X.: The climatic changes of Qarqan river basin and its impact on  
661 the runoff, *Xinjiang Agric. Sci.*, 47 (5), 996-1001, 2010 (in Chinese).

662 Mansur, S. and Ajinisa, T.: An analysis of water resources and it's hydrological characteristics of  
663 Yarkend River Valley, *J. Xinjiang Norm. Univ. (Nat. Sci. Ed.)*, 24(1), 74-78, 2005 (in Chinese).

664 McVicar, T.R., Roderick, M., Donohue, R.J., Li, L.T., Van Niel, T.G., Thomas, A., Grieser, J.,  
665 Jhajharia, D., Himri, Y., Mahowald, N.M., Mescherskaya, A.V., Kruger, A.C., Rehman, S., and  
666 Dinpashoh, Y.: Global review and synthesis of trends in observed terrestrial near-surface wind  
667 speeds: implications for evaporation, *J. Hydrol.*, 416-417, 182-205, 2012.

668 Miralles, D.G., De Jeu, R.A.M., Gash, J.H., Holmes, T.R.H., and Dolman, A.J.: Magnitude and  
669 variability of land evaporation and its components at the global scale, *Hydrol. Earth Syst. Sci.*, 15,  
670 967-981, 2011.

671 Miralles, D.G., Gash, J.H., Holmes, T.R.H., de Jeu, R.A.M, and Dolman, A.J.: Global canopy  
672 interception from satellite observations, *J. Geophys. Res.*, 115, D16122, 2010.

673 Neckel, N., Kropáček, J., Bolch, T., and Hochschild, V.: Glacier mass changes on the Tibetan  
674 Plateau 2003-2009 derived from ICESat laser altimetry measurements, *Environ. Res. Lett.*, 9,  
675 014009(7pp), 2014.

676 Oliveira, P.T.S., Mearing, M.A., Moran, M.S., Goodrich, D.C., Wendland, E., and Gupta, H.V.:  
677 Trends in water balance components across the Brazilian Cerrado, *Water Resour. Res.*, 50,  
678 7100-7114, 2014.

679 Rodell, M., Houser, P.R., Jambor, U., Gottschalck, J., Mitchell, K., Meng, C.-J., Arsenault, K.,  
680 Cosgrove, B., Radakovich, J., Bosilovich, M., Entin, J.K., Walker, P., Lohmann, D., and Toll, D.:  
681 The global land data assimilation system, *B. Am. Meteorol. Soc.*, 85, 381-394, 2004.

682 Rui, H.: README Document for Global Land Data Assimilation System Version 2 (GLDAS-2)  
683 Products, GES DISC, 2011.

684 Saji, N.H., Goswami, B.N., Vinayachandran, P.N., and Yamagata, T.: A dipole mode in the tropical  
685 Indian Ocean, *Nature*, 401, 360-363, 1999.

686 Shen, M.G., Piao, S.L., Jeong, S., Zhou, L.M., Zeng, Z.Z., Ciais, P., Chen, D.L., Huang, M.T., Jin,  
687 C.S., Li, L.Z.X., Li, Y., Myneni, R.B., Yang, K., Zhang, G.X., Zhang, Y.J., and Yao, T.D.:  
688 Evaporative cooling over the Tibetan Plateau induced by vegetation growth, *Proc. Natl. Acad.  
689 Sci. U. S.A.*, 112(30), 9299-9304, 2015.

690 Shi, Y.F., Shen, Y.P., Li, D.L., Zhang, G.W., Ding, Y.J., Hu, R.J., and Kang, E.S.: Discussion on  
691 the present climate change from Warm2dry to Warm2wet in northwest China, *Quat. Sci.*, 23(2),  
692 152-164, 2003 (in Chinese).

693 Shepard, D.S.: Computer mapping: the SYMAP interpolation algorithm. *Spatial Statistics and  
694 Models*, G.L. Gaile and C.J. Willmott, Eds., D. Reidel, 133-145, 1984.

695 Sun, B., Mao, W., Feng, Y., Chang, T., Zhang, L., and Zhao, L.: Study on the change of air  
696 temperature, precipitation and runoff volume in the Yarkant River basin, *Arid Zone Res.*, 23(2),  
697 203-209, 2006 (in Chinese).

698 Takala, M., Luoju, K., Pulliainen, J., Derksen, C., Lemmetyinen, J., Kärnä J.-P., Koskinen, J., and  
699 Bojkov, B.: Estimating northern hemisphere snow water equivalent for climate research through  
700 assimilation of spaceborne radiometer data and ground-based measurements, *Remote*

701 Sens. Environ., 115 (12), 3517-3529, 2011.

702 Tapley, B.D., Bettadpur, S., Watkins, M., and Randerhager, C.: The gravity recovery and climate  
703 experiment: mission overview and early results, *Geophys. Res. Lett.*, 31, L09607, 2004.

704 Tian, L., Yao, T., MacClune, K., White, J.W.C., Schilla, A., Vaughn, B., Vachon, R., and  
705 Ichiyonagi, K.: Stable isotopic variations in west China: a consideration of moisture sources, *J.*  
706 *Geophys. Res. Atmos.*, 112, D10112, 2007.

707 Tucker, C.J., Pinzon, J.E., Brown, M.E., Slayback, D., Pak, E.W., Mahoney, R., Vermote, E., and  
708 El Saleous, N.: An extended AVHRR 8 km NDVI data set compatible with MODIS and SPOT  
709 vegetation NDVI data, *Int. J. Remote Sens.*, 26(20), 4485-4498, 2005.

710 von Storch, H.: Misuses of statistical analysis in climate research, In *Analysis of Climate*  
711 *Variability: Applications of Statistical Techniques*, Springer-Verlag: Berlin, 11-26, 1995.

712 Wang, A. and Zeng, X.: Evaluation of multireanalysis products within site observations over the  
713 Tibetan Plateau, *J. Geophys. Res.*, 117, D05102, 2012.

714 Wang, L., Sun, L.T., Shrestha, M., Li, X.P., Liu, W.B., Zhou, J., Yang, K., Lu, H., and Chen, D.L.:  
715 Improving snow process modeling with satellite-based estimation of  
716 near-surface-air-temperature lapse rate, *J. Geophys. Res. Atmos.*, 121, 12005-12030, 2016.

717 Xia, Y., Mitchell, K., Ek, M., Cosgrove, B., Sheffield, J., Luo, L., Alonge, C., Wei, H., Meng, J.,  
718 Livneh, B., and Duang, Q.: Continental-scale water and energy flux analysis and validation for  
719 North American Land Data Assimilation System project phase 2 (NLDAS-2): 2. Validation of  
720 model-simulated streamflow, *J. Geophys. Res. Atmos.*, 117(D3), D03110, 2012.

721 Xiang, L., Wang, H., Steffen, H., Wu, P., Jia, L., Jiang, L., and Shen, Q.: Groundwater storage  
722 changes in the Tibetan Plateau and adjacent areas revealed from GRACE satellite gravity data,  
723 *Earth Planet. Sci. Lett.*, 449, 228-239, 2016.

724 Xu, L.: The land surface water and energy budgets over the Tibetan Plateau, Available from  
725 Nature Precedings < <http://hdl.handle.net/10101/npre.2011.5587.1>>, 2011.

726 Xue, B.L., Wang, L., Yang, K., Tian, L., Qin, J., Chen, Y., Zhao, L., Ma, Y., Koike, T., Hu, Z., and  
727 Li, X.P.: Modeling the land surface water and energy cycle of a mesoscale watershed in the  
728 central Tibetan Plateau with a distributed hydrological model, *J. Geophys. Res. Atmos.*, 118,  
729 8857-8868, 2013.

730 Yao, Z., Duan, R., and Liu, Z.: Changes in precipitation and air temperature and its impacts on  
731 runoff in the Nujiang River basins. *Resour. Sci.* 34(2), 202-210, 2012 (in Chinese)

732 Yang, K., Qin, J., Zhao, L., Chen, Y.Y., Tang, W.J., Han, M.L., Lazhu, Chen, Z.Q., Lv, N., Ding,  
733 B.H., Wu, H., and Lin, C.G.: A multi-scale soil moisture and freeze-thaw monitoring network  
734 on the third pole, *Bull. Am. Meteorol. Soc.*, 94,1907-1916, 2013.

735 Yang, K., Wu, H., Qin, J., Lin, C.G., Tang, W.J., and Chen, Y.Y.: Recent climate changes over the  
736 Tibetan Plateau and their impacts on energy and water cycle: a review, *Glob. Planet Change*,  
737 112, 79-91, 2014.

738 Yao, T.D., Thompson, L., Yang, W., Yu, W.S., Gao, Y., Guo, X.J., Yang, X.X., Duan, K.Q., Zhao,  
739 H.B., Xu, B.Q., Pu, J.C., Lu, A.X., Xiang, Y., Kattel, D.B., and Joswiak, D.: Different glacier  
740 status with atmospheric circulations in Tibetan Plateau and surroundings, *Nat. Clim. Change*, 2,  
741 1-5, 2012.

742 Yao, Y.J., Zhao, S.H., Zhang, Y.H., Jia, K., and Liu, M.: Spatial and decadal variations in potential  
743 evapotranspiration of China based on reanalysis datasets during 1982-2010, *Atmosphere*, 5,  
744 737-754, 2014.

745 Yin, G., Hu, Z.Y., Chen, X., and Tiyyip, T.: Vegetation dynamics and its response to climate change  
746 in Central Asia, *J. Arid Land*, 8, 375, 2016.

747 Yu, J., Zhang, G., Yao, T., Xie, H., Zhang, H., Ke, C., and Yao, R.: Developing daily cloud-free  
748 snow composite products from MODIS Terra-Aqua and IMS for the Tibetan Plateau, *IEEE*  
749 *Trans. Geosci. Remote Sens.*, 54(4), 2171-2180, 2015.

750 Yue, S., Pilon, P., Phinney, B., Cavadias, G.: The influence of autocorrelation on the ability to  
751 detect trend in hydrological series, *Hydrol. Process.*, 16(9), 1807-1829, 2002.

752 Zhang, D., Liu, X., Zhang, Q., Liang, K., and Liu, C.: Investigation of factors affecting  
753 inter-annual variability of evapotranspiration and streamflow under different climate conditions.  
754 *J. Hydrol.*, doi:10.1016/j.jhydrol.2016.10.047, 2016.

755 Zhang, G., Xie, H., Yao, T., Liang, T., and Kang, S.: Snow cover dynamics of four lake basins  
756 over Tibetan Plateau using time series MODIS data (2001-2100), *Water Resour. Res.*, 48(10),  
757 W10529, 2012.

758 Zhang, K., Kimball, J.S., Nemani, R.R., and Running, S.W.: A continuous satellite-derived global  
759 record of land surface evapotranspiration from 1983 to 2006, *Water Resour. Res.*, 46(9),

760 W09522, 2010.

761 Zhang, L., Su, F., Yang, D., Hao, Z., and Tong, K.: Discharge regime and simulation for the  
762 upstream of major rivers over Tibetan Plateau, *J. Geophys. Res. Atmos.*, 118(15), 8500-8518,  
763 2013.

764 Zhang, Q., Li, J., Singh, V., and Xu, C.: Copula-based spatial-temporal patterns of precipitation  
765 extremes in China, *Int. J. Climatol.*, 33, 1140-1152, 2013.

766 Zhang, X., Tang, Q., Pan, M., and Tang, Y.: A long-term land surface hydrologic fluxes and states  
767 dataset for China, *J. Hydrometeorol.*, 15, 2067-2084, 2014.

768 Zhang, Y., Peña-Arancibia, J.L., McVicar, T.R., Chiew, F.H.S., Vaze, J., Liu, C.M., Lu, X.J.,  
769 Zheng, H.X., Wang, Y.P., Liu, Y.Y., Miralles, D.G., and Pan, M.: Multi-decadal trends in global  
770 terrestrial evapotranspiration and its components, *Scientific Reports*, 6, 19124, 2016.

771 Zhang, Y., Liu, C., Tang, Y., and Yang, Y.: Trend in pan evaporation and reference and actual  
772 evapotranspiration across the Tibetan Plateau, *J. Geophys. Res.*, 112, D12110, 2007.

773 Zhou, C., Jia, S., Yan, H., and Yang, G.: Changing trend of water resources in Qinghai Province  
774 from 1956 to 2000, *J. Glaciol. Geocryol.*, 27(3), 432-437, 2005 (in Chinese).

775 Zhou, J., Wang, L., Zhang, Y.S., Guo, Y.H., Li, X.P., and Liu, W.B.: Exploring the water storage  
776 changes in the largest lake (Selin Co) over the Tibetan Plateau during 2003-2012 from a  
777 basin-wide hydrological modeling., *Water Resour. Res.*, 51, 8060-8086, 2015.

778 Zhou, S.Q., Kang, S., Chen, F., and Joswiak, D.R.: Water balance observations reveal significant  
779 subsurface water seepage from Lake Nam Co., south-central Tibetan Plateau., *J. Hydrol.*, 491,  
780 89-99, 2013.

781 Zhou, S.Q., Wang, Z., and Joswiak, D.R.: From precipitation to runoff: stable isotopic fractionation  
782 effect of glacier melting on a catchment scale, *Hydrol. Process.*, 28(8), 3341-3349, 2014.

783 Zhu, Y., Chen, J., Chen, G.: Runoff variation and its impacting factors in the headwaters of the  
784 Yangtze River in recent 32 years, *J. Yangtze River Sci. Res. Inst.*, 28(6), 1-4, 2011 (in Chinese ).

785 **Table 1:** Main features of the 18 used TP river basins. GA% and SC% represent the percentages of multiyear-mean glacier cover and snow cover in each basin.  
786 The glacier and snow cover data are extracted, respectively, from the Second Glacier Inventory Dataset of China and the daily TP snow cover dataset  
787 (2005-2013)  
788

No.	Station	Altitude (m)	River name	Drainage area (km <sup>2</sup> )	Multiyear-mean (1982-2011) and basin-averaged parameters						
					Q (mm/yr)	Prec. (mm/yr)	Temp.(°C/yr)	NDVI	LAI	GA%	SC%
01	Kulukelangan	2000	Yerqiang	32880.00	158.60	128.34	-5.68	0.05	0.03	10.97	35.03
02	Tongguziluoke	1650	Yulongkashi	14575.00	151.56	134.04	-4.07	0.06	0.04	23.27	35.95
03	Numaitilangan	1880	Keliya	7358.00	103.18	137.14	-4.78	0.06	0.03	10.86	29.16
04	Zelingou	4282	Bayin	5544.00	41.42	340.68	-4.98	0.13	0.09	0.09	21.22
05	Gadatan	3823	Yellow	7893.00	200.95	566.01	-4.60	0.34	0.54	0.13	14.94
06	Xining	3225	Yellow	9022.00	99.90	503.74	0.97	0.36	0.70	0.00	10.06
07	Tongren	3697	Yellow	2832.00	149.36	533.25	-1.37	0.39	0.83	0.00	9.42
08	Tainaihai	2632	Yellow	121972.00	159.48	540.32	-2.40	0.34	0.72	0.09	15.89
09	Huangheyan	4491	Yellow	20930.00	31.18	386.42	-4.81	0.23	0.61	0.00	17.25
10	Jimai	4450	Yellow	45015.00	85.50	441.48	-4.16	0.26	0.52	0.00	20.05
11	Yajiang	2599	Yalong	67514.00	237.66	717.05	-0.23	0.43	0.80	0.15	18.36
12	Zhimenda	3540	Yangtze	137704.00	96.23	405.66	-4.83	0.20	0.26	0.96	17.87
13	Jiaoyuqiao	3000	Salween	72844.00	364.26	620.88	-1.89	0.29	0.44	2.02	23.73
14	Pangduo	5015	Brahmaputra	16459.00	348.31	544.59	-1.53	0.27	0.33	1.66	23.33
15	Tangjia	4982	Brahmaputra	20143.00	350.61	555.17	-1.89	0.27	0.34	1.39	21.83
16	Gongbujiangda	4927	Brahmaputra	6417.00	586.96	692.06	-4.24	0.27	0.36	4.12	25.99
17	Nuxia	2910	Brahmaputra	191235.00	307.38	401.35	-0.73	0.22	0.25	1.90	13.50
18	Yangcun	3600	Brahmaputra	152701.00	163.25	349.91	-0.87	0.19	0.18	1.28	10.52

789  
790



791 **Table 2:** Overview of multi-source datasets applied in this study

792

Data category	Data source	Spatial resolution	Temporal resolution	Available period used	Reference
Runoff (Q)	Observed, National Hydrology Almanac of China	—	Daily	1982-2011	—
	VIC_IGSNRR simulated	0.25°	Daily	1982-2011	Zhang et al. (2014)
Precipitation (P)	Observed, CMA	0.5°	Monthly	1982-2011	—
	TRMM 3B43 V7	0.25°	Monthly	2000-2011	Huffman et al. (2012)
	IGSNRR forcing	0.25°	Daily	1982-2011	Zhang et al. (2014)
Temperature (Temp.)	Observed, CMA	0.5°	Monthly	2000-2011	—
Terrestrial storage change (ΔS)	GRACE-CSR	Approx.300-400 km	Monthly	2002-2011	Tapley et al. (2004)
	GRACE-GFZ	Approx.300-400 km	Monthly	2002-2011	Tapley et al. (2004)
	GRACE-JPL	Approx.300-400 km	Monthly	2002-2011	Tapley et al. (2004)
Potential evaporation (PET)	CRU	0.5°	Monthly	1982-2011	Harris et al. (2013)
Actual evaporation (ET)	MTE_E	0.5°	Monthly	1982-2011	Jung et al. (2010)
	VIC_E	0.25°	Daily	1982-2011	Zhang et al. (2014)
	GLEAM_E	0.25°	Daily	1982-2011	Miralles et al. (2011)
	PML_E	0.5°	Monthly	1982-2011	Zhang Y et al. (2016)
	Zhang_E	8 km	Monthly	1983-2006	Zhang et al. (2010)
	GNoah_E	1.0°	3 hourly	1982-2011	Rui (2011)
NDVI	GIMMS NDVI dataset	8 km	15 daily	1982-2011	Tucker et al. (2005)
LAI	GLASS LAI Product	0.05°	8 daily	1982-2011	Liang and Xiao (2012)
Snow Cover	TP Snow composite Products	500 m	Daily	2005-2013	Zhang et al. (2012)
SWE	VIC_IGSNRR simulated	0.25°	Daily	1982-2011	Zhang et al. (2014)
	GlobSnow-2 Product	25 km	Daily	1982-2011	Takala et al. (2011)

793

794 **Table 3:** Contribution of glacier-melt to discharge in eighteen basins (“—” shows no glacier influences, “—\*” shows the percentage is empirically estimated  
795 through the relation between lacier area ratio and glacier melt for basins in which the glacier melt contribution has been reported in the literatures)  
796

Basin	Contributions of glacier-melt to discharge (%)	Reference
Kulukelangan	62.73	Mansur and Ajnisa (2005)
Tongguziluoke	64.90	Liu J et al. (2016)
Numaitilangan	71	Chen (1988)
Zelingou	—	—
Gadatan	—	—
Xining	—	—
Tongren	—	—
Tainaihai	0.80	Zhang et al. (2013)
Huangheyuan	—	—
Jimai	—	—
Yajiang	1.40	—*
Zhimenda	6.50	Zhang et al. (2013)
Jiaoyuqiao	4.80	Zhang et al. (2013)
Nuxia	11.60	Zhang et al. (2013)
Pangduo	10.13	—*
Tangjia	8.49	—*
Gongbujiangda	25.15	—*
Yangcun	7.81	—*

797  
798  
799

800 **Table 4:** Nonparametric trends for different ET estimates during the period 1982-2006 detected by modified Mann-Kendall test, the bold number showed the  
 801 detected trend is statistically significant at the 0.05 level

802	Basin	ET <sub>wb</sub>	GLEAM_E	VIC_E	Zhang_E	PML_E	MET_E	GNoah_E
804	Kulukelangan	<b>-0.09</b>	0.09	<b>0.18</b>	–	0.03	-0.01	0.07
	Tongguziluoke	-0.02	0.10	<b>0.13</b>	–	0.03	<b>-0.08</b>	0.19
805	Numaitilangan	0.04	<b>0.10</b>	0.14	–	0.14	<b>-0.10</b>	0.22
	Zelingou	<b>0.13</b>	<b>0.23</b>	0.11	<b>0.09</b>	0.04	<b>0.06</b>	0.02
806	Gadatan	-0.09	0.25	0.070	-0.10	-0.01	<b>0.06</b>	-0.07
	Xining	-0.06	<b>0.54</b>	0.01	-0.08	0.01	0.02	-0.06
807	Tongren	-0.06	<b>0.34</b>	-0.15	<b>-0.17</b>	0.07	0.02	0.13
	Tainaihai	0.06	<b>0.28</b>	-0.03	<b>-0.11</b>	0.04	<b>0.05</b>	0.04
808	Huangheyang	0.08	<b>0.19</b>	-0.01	<b>-0.10</b>	<b>0.08</b>	<b>0.05</b>	<b>0.10</b>
	Jimai	-0.07	<b>0.23</b>	-0.01	-0.08	0.03	<b>0.05</b>	0.10
809	Yajiang	0.17	<b>0.26</b>	<b>0.06</b>	<b>-0.21</b>	-0.01	0.03	-0.02
	Zhimenda	0.11	<b>0.28</b>	0.10	0.01	0.07	<b>0.04</b>	0.07
810	Jiaoyuqiao	<b>0.18</b>	<b>0.28</b>	0.10	<b>-0.11</b>	0.05	<b>0.05</b>	0.07
	Nuxia	<b>-0.09</b>	<b>0.25</b>	0.09	<b>-0.10</b>	<b>0.12</b>	<b>0.04</b>	0.10
811	Pangduo	0.05	<b>0.28</b>	<b>0.17</b>	<b>-0.07</b>	0.07	<b>0.07</b>	<b>0.11</b>
	Tangjia	0.09	<b>0.26</b>	<b>0.17</b>	<b>-0.09</b>	<b>0.20</b>	<b>0.06</b>	<b>0.12</b>
812	Gongbujiangda	-0.26	0.12	0.13	<b>-0.16</b>	<b>0.19</b>	0.01	<b>0.15</b>
	Yangcun	0.03	<b>0.28</b>	0.08	<b>-0.06</b>	0.10	0.04	0.09

813

814

815 **Figure captions:**

816 **Figure1.** Map of river basins and hydrological gauging stations (green dots) over the  
817 Tibetan Plateau (TP) used in this study. The grey shading shows the topography of TP  
818 in meters above the sea level and the blue shading exhibits the glaciers distribution in  
819 TP extracted from the Second Glacier Inventory Dataset of China.

820 **Figure 2.** Comparison of VIC\_IGSNRR simulated and observed monthly runoff for  
821 Tangnaihai and Panduo stations (a and b) as well as (c) basin-averaged monthly  
822 TRMM, CMA gridded and IGSNRR forcing precipitations for the smallest basin  
823 (Tongren station) over the period 1982-2011. (d) shows the comparison of TRMM  
824 (blue) and IGSNRR forcing (red) precipitations against CMA gridded precipitation for  
825 18 river basins over TP during the period 2000-2011.

826 **Figure 3.** Comparison of different ET products against the calculated ET through the  
827 water balance method ( $ET_{wb}$ ) for 18 TP basins. The boxplot of annual estimates of  
828 different ET products for 18 TP basins are shown in (a) while the correlation  
829 coefficients and root-mean-square-errors (RMSEs, mm/month) for each ET product  
830 relatively to  $ET_{wb}$  are exhibited in (b).

831 **Figure 4.** General water and energy status (a. the perspective of Budyko framework)  
832 and their relationships with glacier (b) and vegetation (c and d) for eighteen TP river  
833 basins (1983-2006). The ET used in this figure is calculated from the bias-corrected  
834 water balance method.

835 **Figure 5.** Seasonal cycles (1982-2011) of water budget components in westerlies-  
836 dominated (column 1), East Asian monsoon-dominated (columns 2-4) and Indian  
837 monsoon-dominated (columns 5-6) TP basins.

838 **Figure 6.** Seasonal cycles (1982-2011) of air temperature and vegetation parameters  
839 in westerlies-dominated (column 1), East Asian monsoon-dominated (columns 2-4)  
840 and Indian monsoon-dominated (columns 5-6) TP basins.

841 **Figure 7.** Seasonal cycles (1982-2011) of snow cover and snow water equivalent  
842 (SWE) in westerlies-dominated (column 1), East Asian monsoon-dominated (columns  
843 2-4) and Indian monsoon-dominated (columns 5-6) TP basins. The snow cover was

844 extracted from cloud free snow composite product during the period 2005-2013. It  
845 should also be noted that the GlobSnow data are not available for some basins.

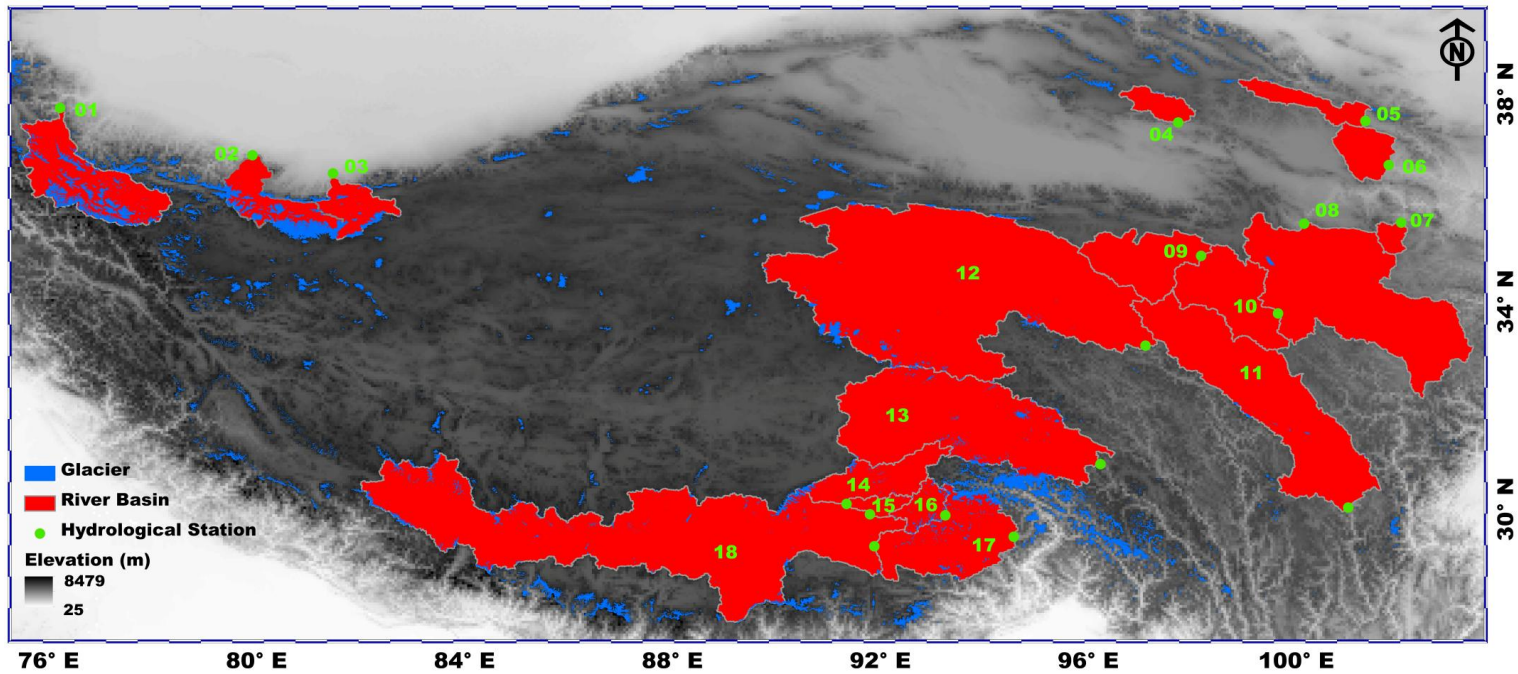
846 **Figure 8.** Sen's slopes of water budget components and vegetation parameters in  
847 westerlies-dominated TP basins during the period of 1982-2011. The double red stars  
848 showed that the trend was statistically significant at the 0.05 level.

849 **Figure 9.** Linear and non-parametric trends of westerly, Indian monsoon and East  
850 Asian summer monsoon during the period 1982-2011 revealed prospectively by the  
851 Asian Zonal Circulation Index, Indian Ocean Dipole Mode Index and East Asian  
852 Summer Monsoon Index.

853 **Figure 10.** Similar to Figure 8 but for East Asian monsoon-dominated TP basins. It  
854 should be noted that the GlobSnow data are not available for some basins. The double  
855 red stars showed that the trend was statistically significant at the 0.05 level.

856 **Figure 11.** Similar to Figure 8 but for Indian monsoon-dominated TP basins. It should  
857 be noted that the GlobSnow data are not available for some basins. The double red  
858 stars showed that the trend was statistically significant at the 0.05 level.

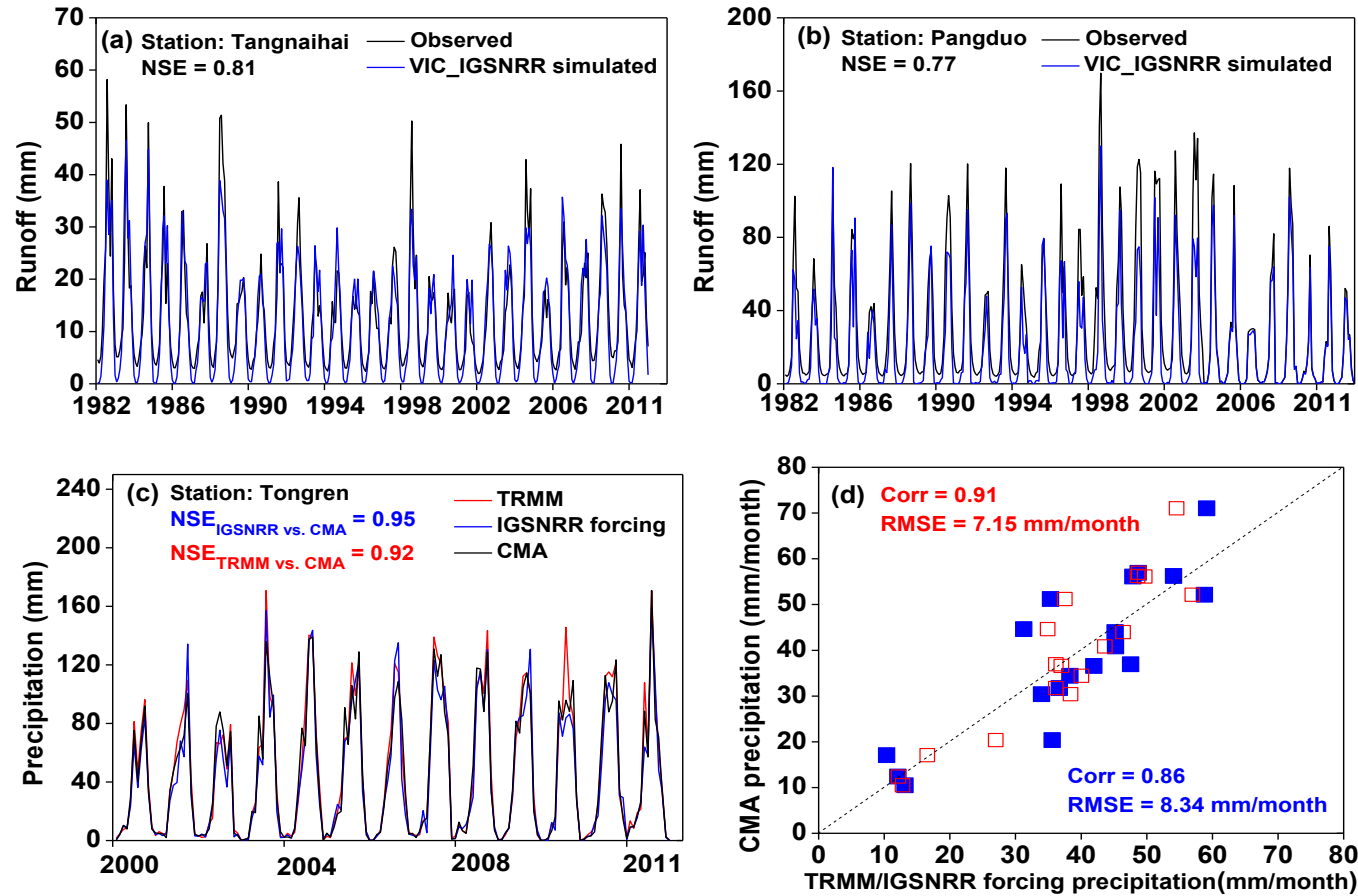
859 **Figure 1.** Map of river basins and hydrological gauging stations (green dots) over the Tibetan Plateau (TP) used in this study. The grey shading shows the  
860 topography of TP in meters above the sea level and the blue shading exhibits the glaciers distribution in TP extracted from the Second Glacier Inventory Dataset of  
861 China.



862

863

864 **Figure 2.** Comparison of VIC\_IGSNRR simulated and observed monthly runoff for Tangnaihai and Panduo stations (a and b) as well as (c) basin-averaged  
 865 monthly TRMM, CMA gridded and IGSNRR forcing precipitations for the smallest basin (Tongren station) over the period 1982-2011. (d) shows the comparison of  
 866 TRMM (blue) and IGSNRR forcing (red) precipitations against CMA gridded precipitation for 18 river basins over TP during the period 2000-2011.

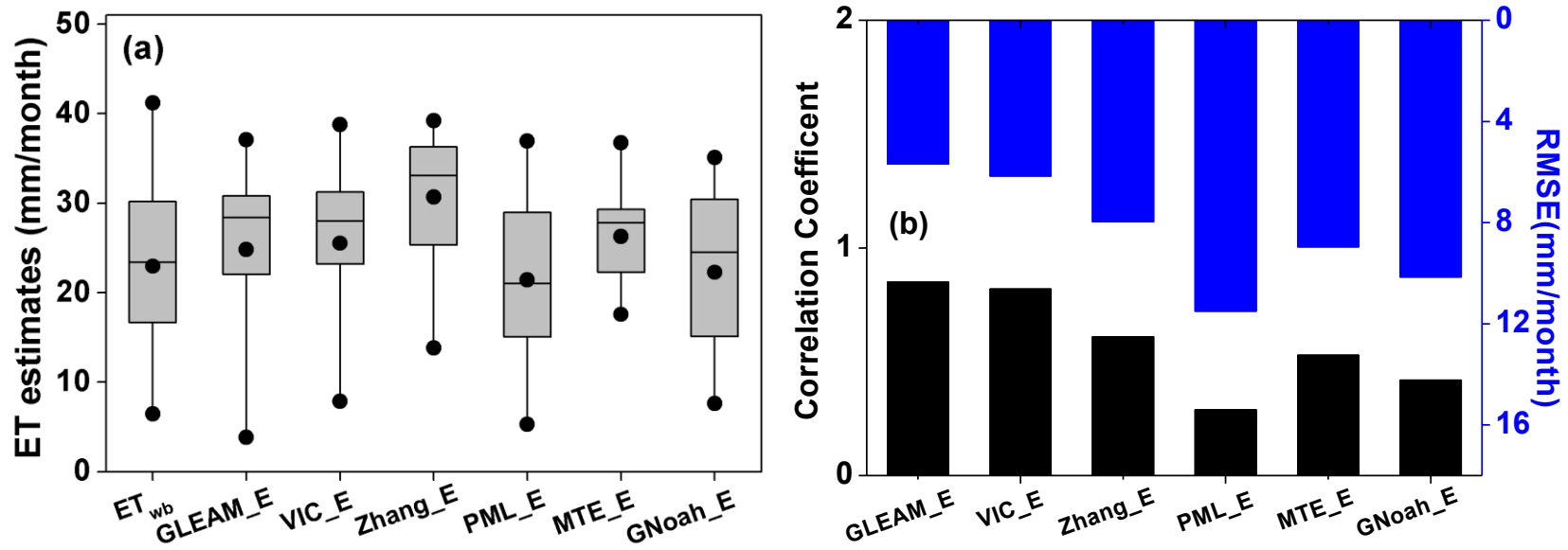


867

868

869

870 **Figure 3.** Comparison of different ET products against the calculated ET through the water balance ( $ET_{wb}$ ) for 18 river basins over the Tibetan Plateau. The  
 871 boxplot of annual estimates of different ET products for 18 TP basins are shown in (a) while the correlation coefficients and root-mean-square-errors (RMSEs,  
 872 mm/month) for each ET product relatively to  $ET_{wb}$  are exhibited in (b).

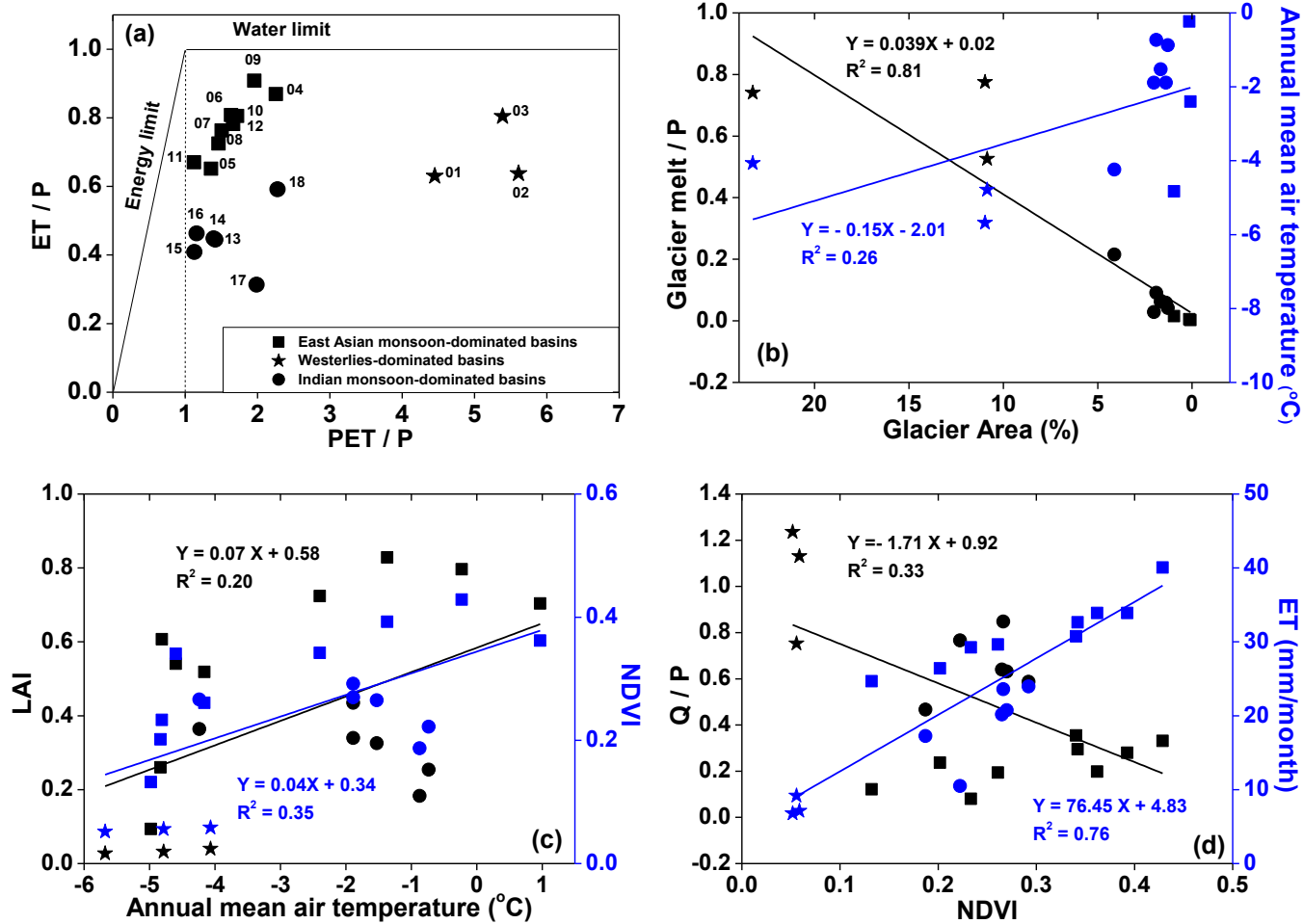


873

874



875 **Figure 4.** General water and energy status (a. the perspective of Budyko framework) and their relationships with glacier (b) and vegetation (c and d) for eighteen  
 876 TP river basins (1983-2006). The ET used in this figure is calculated from the bias-corrected water balance method.

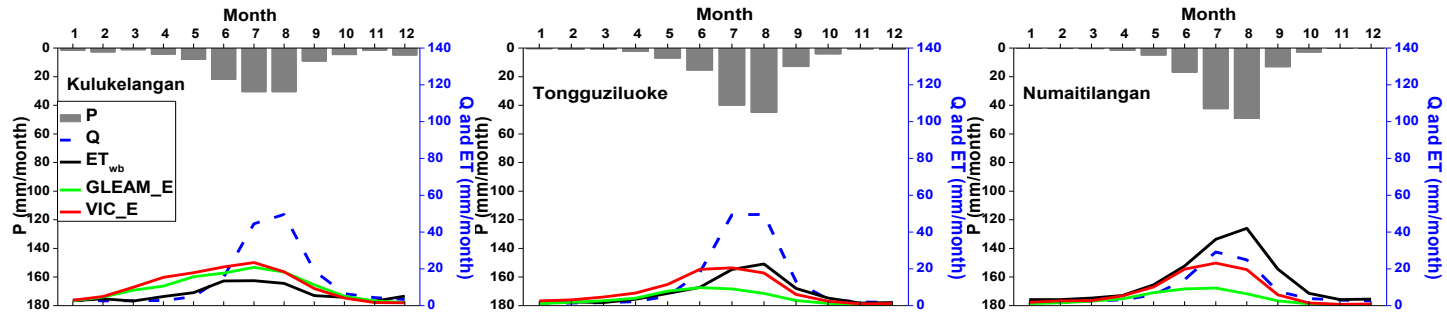


877

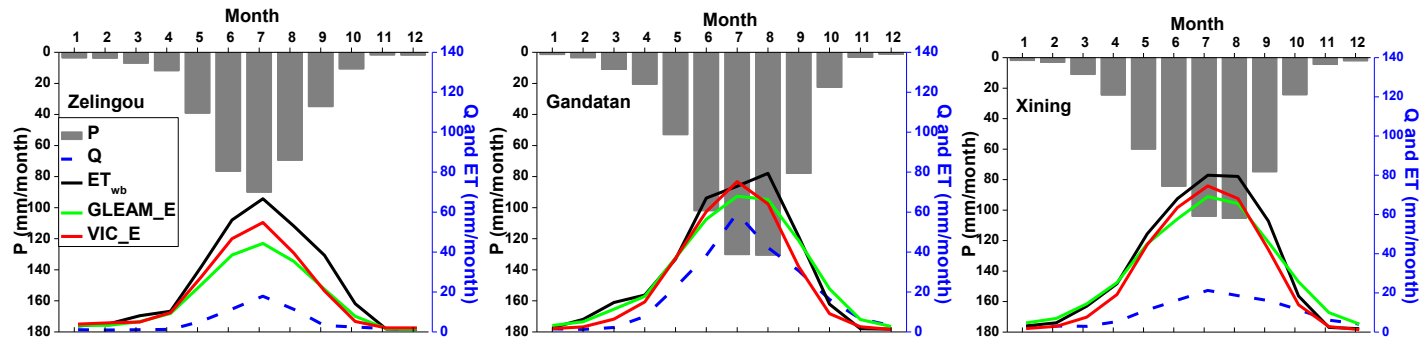
878

879 **Figure 5.** Seasonal cycles (1982-2011) of water budget components in westerlies-dominated (column 1), East Asian monsoon-dominated (columns 2-4) and Indian  
 880 monsoon-dominated (columns 5-6) TP basins.

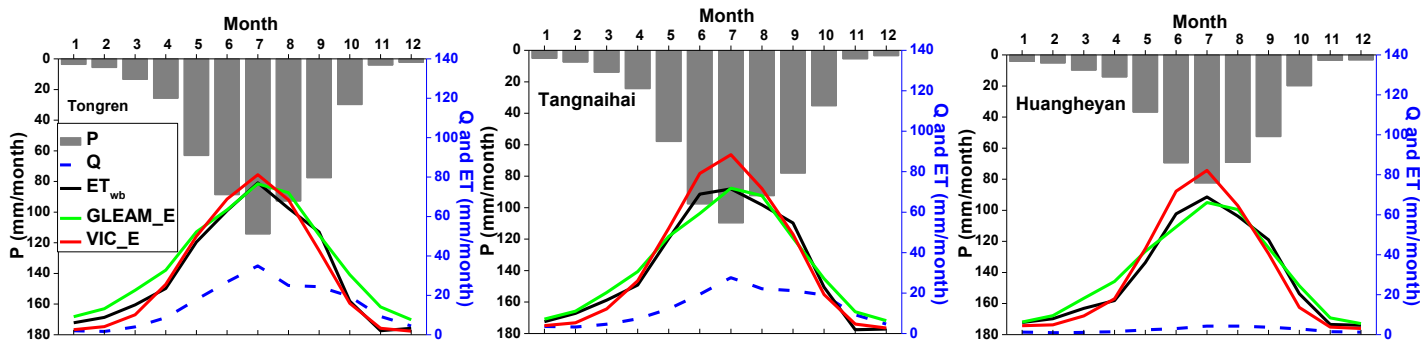
881



882



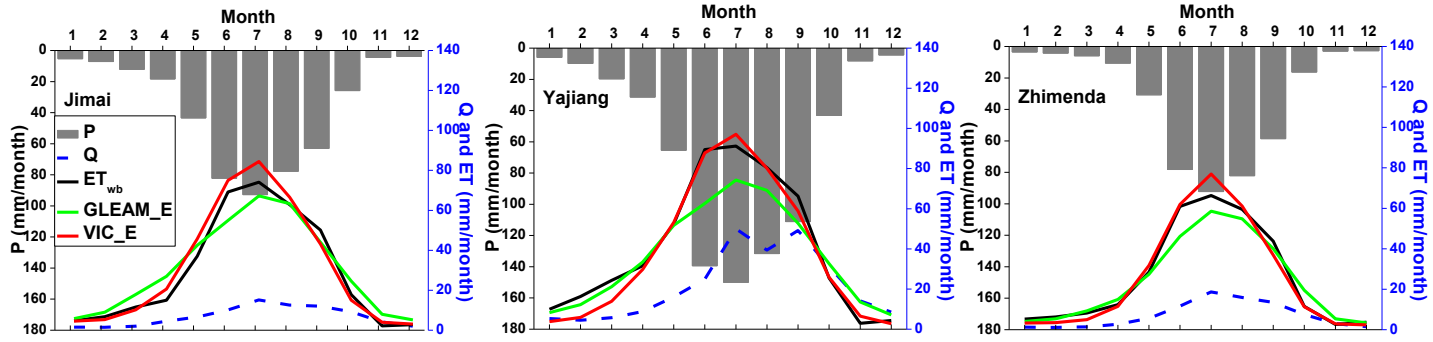
883



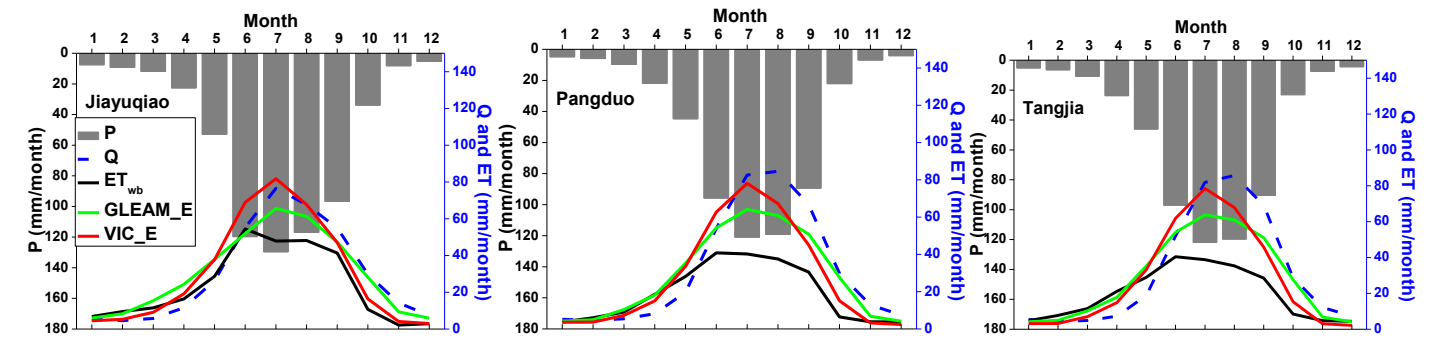
884

Figure 5: (continued)

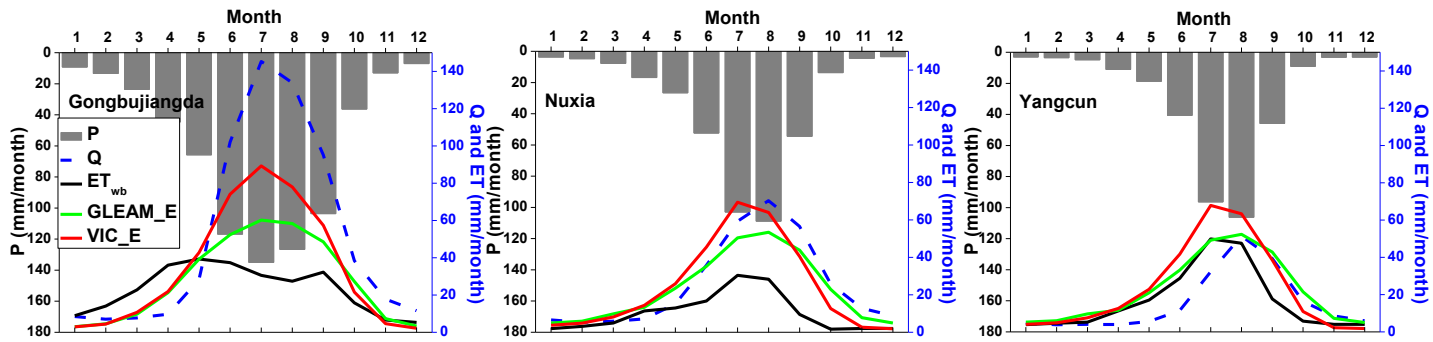
885



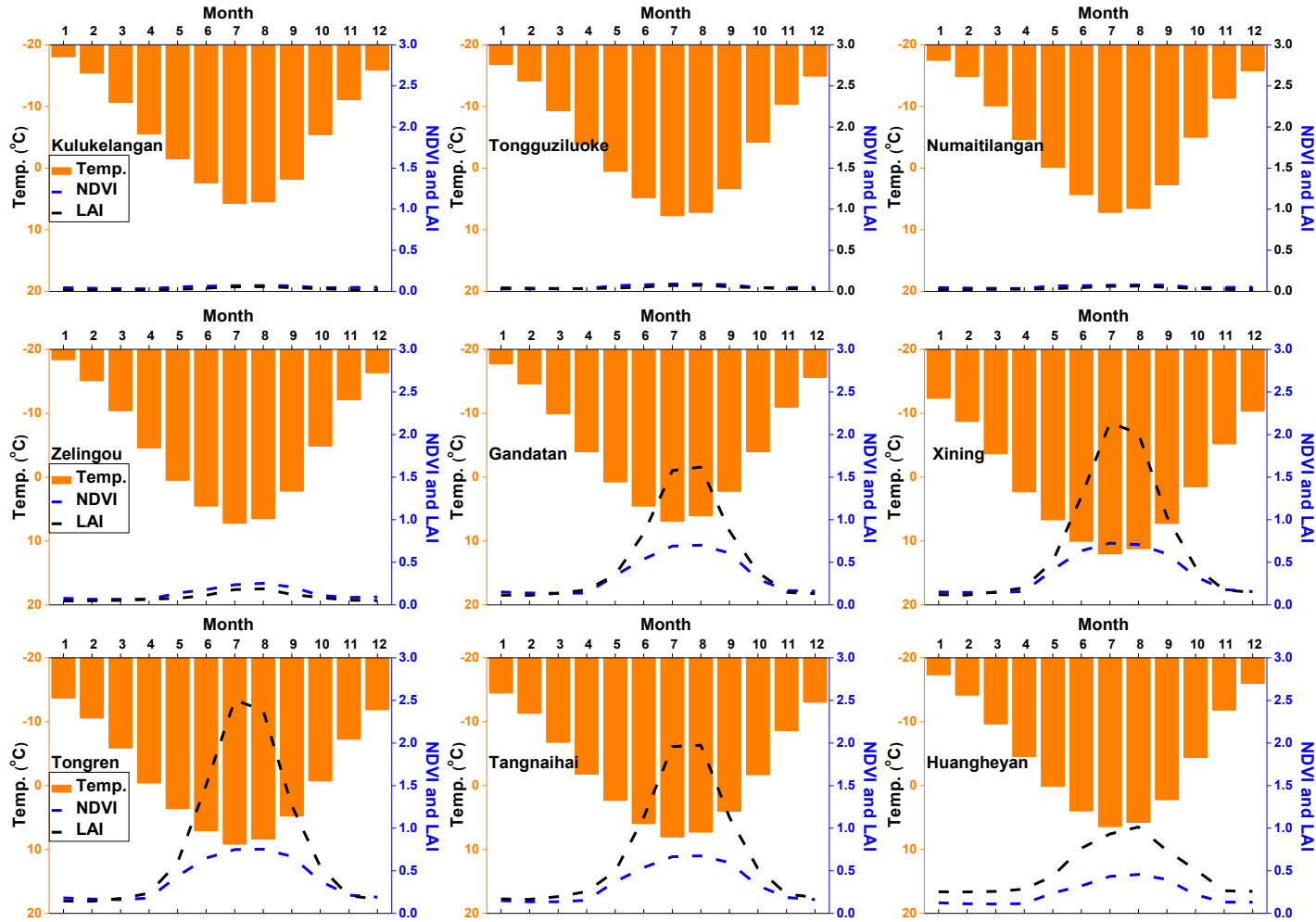
886



887



888 **Figure 6.** Seasonal cycles (1982-2011) of air temperature and vegetation parameters in westerlies-dominated (column 1), East Asian monsoon-dominated (columns  
 889 2-4) and Indian monsoon-dominated (columns 5-6) TP basins.



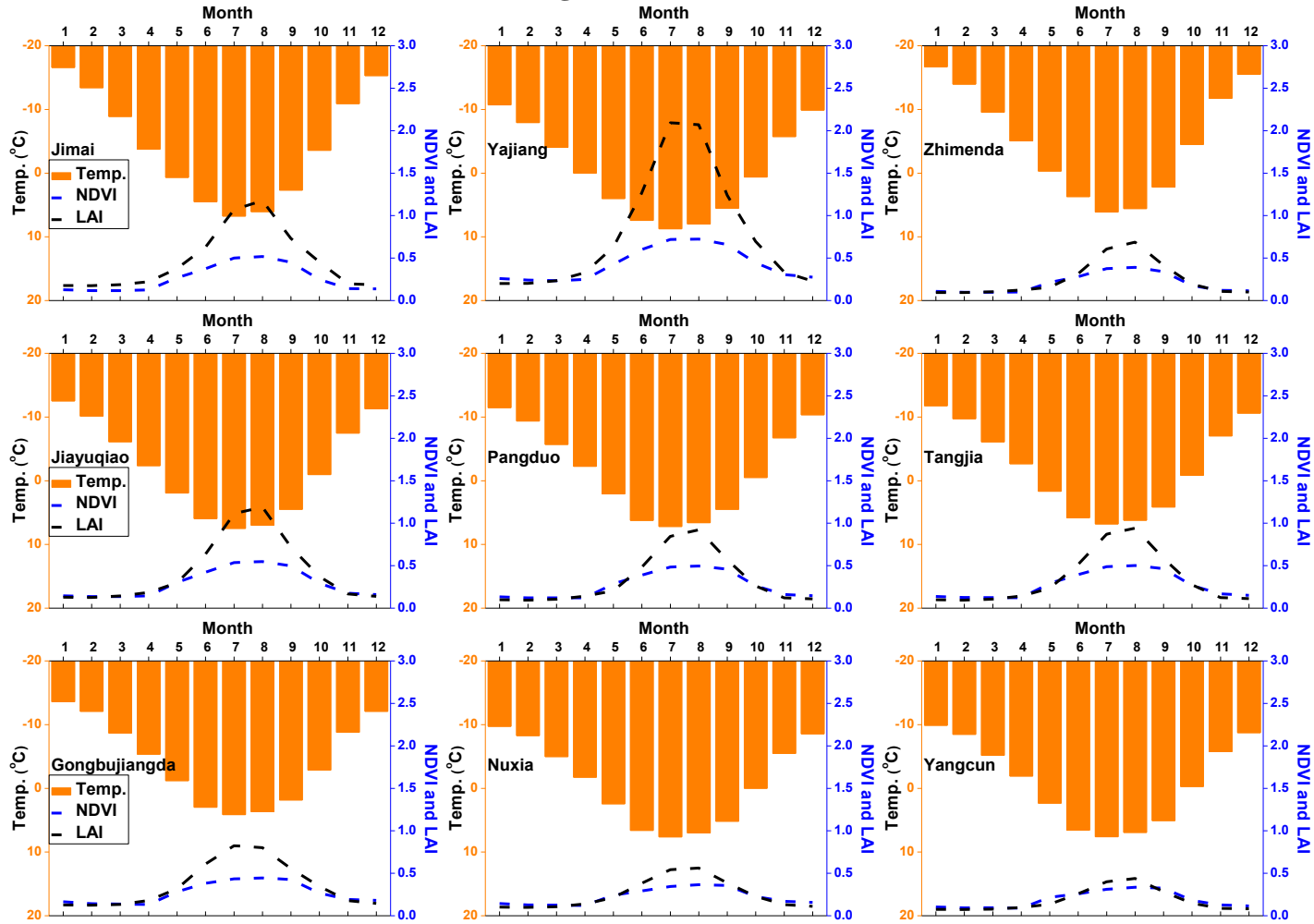
890

891

892

893

Figure 6: (continued)



894

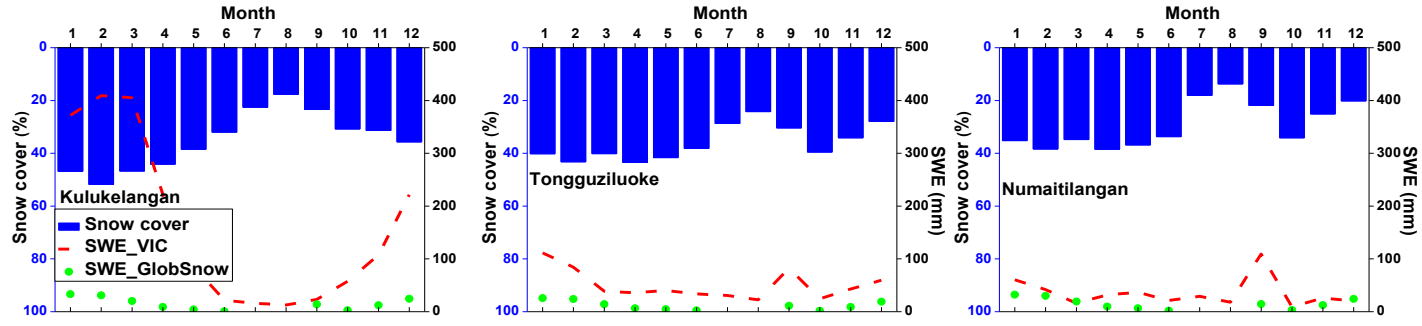
895

896

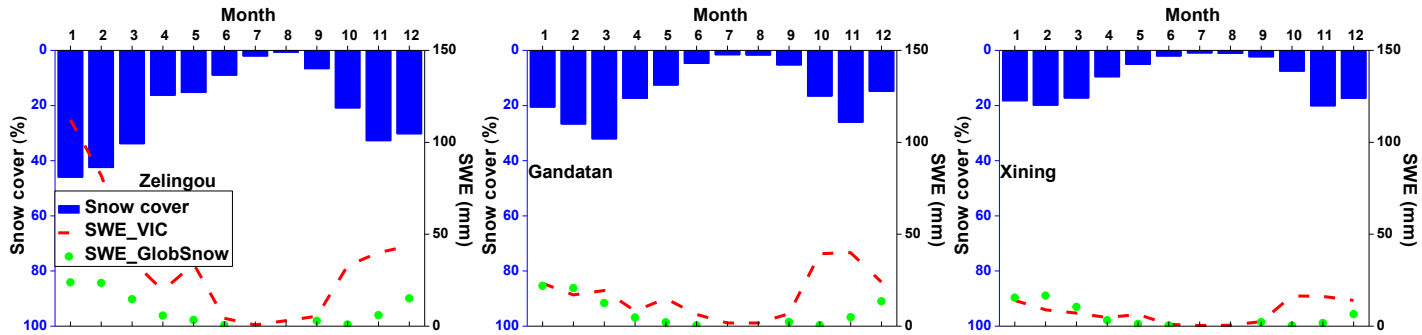
897

898 **Figure 7.** Seasonal cycles (1982-2011) of snow cover and snow water equivalent (SWE) in westerlies-dominated (column 1), East Asian monsoon- dominated  
899 (columns 2-4) and Indian monsoon-dominated (columns 5-6) TP basins. The snow cover was extracted from cloud free snow composite product during the period  
900 2005-2013. It should also be noted that the GlobSnow data are not available for some basins.  
901

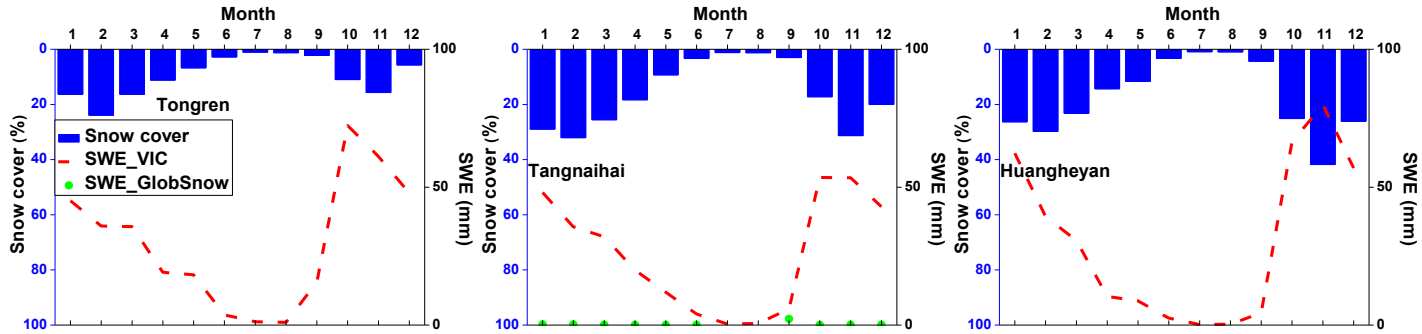
902



903



904

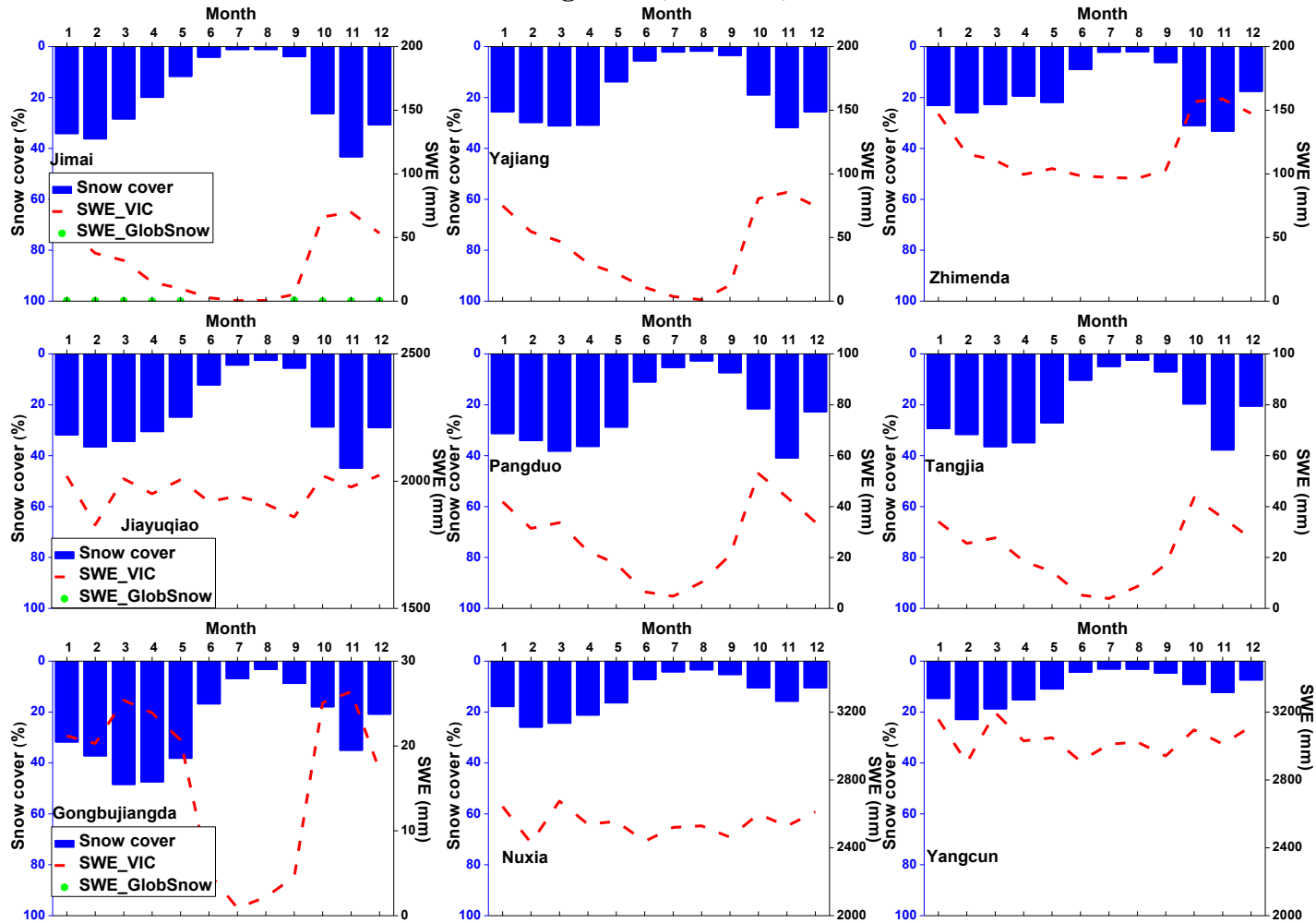


905

906

907

Figure 7: (continued)



908

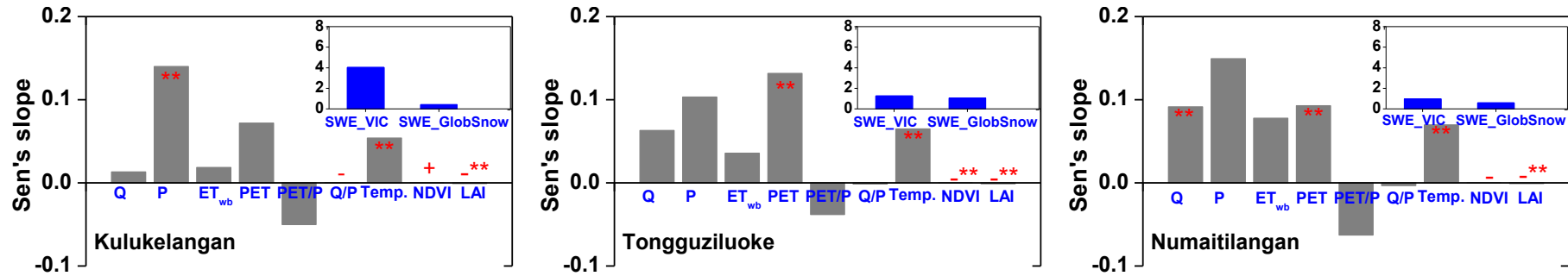
909

910

911

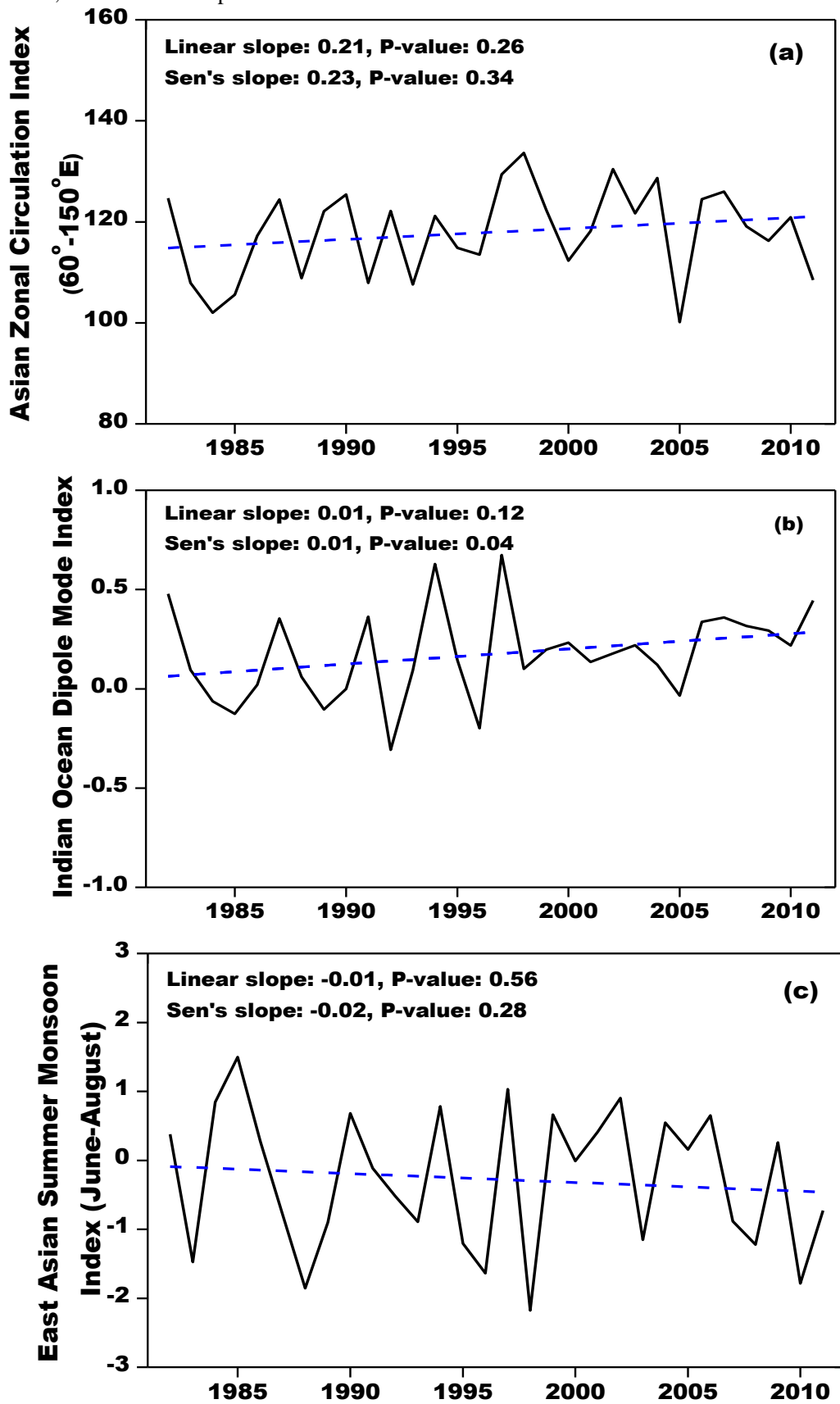


912 **Figure 8.** Sen's slopes of water budget components and vegetation parameters in westerlies-dominated TP basins during the period of 1982-2011. The double red  
 913 stars showed that the trend was statistically significant at the 0.05 level.

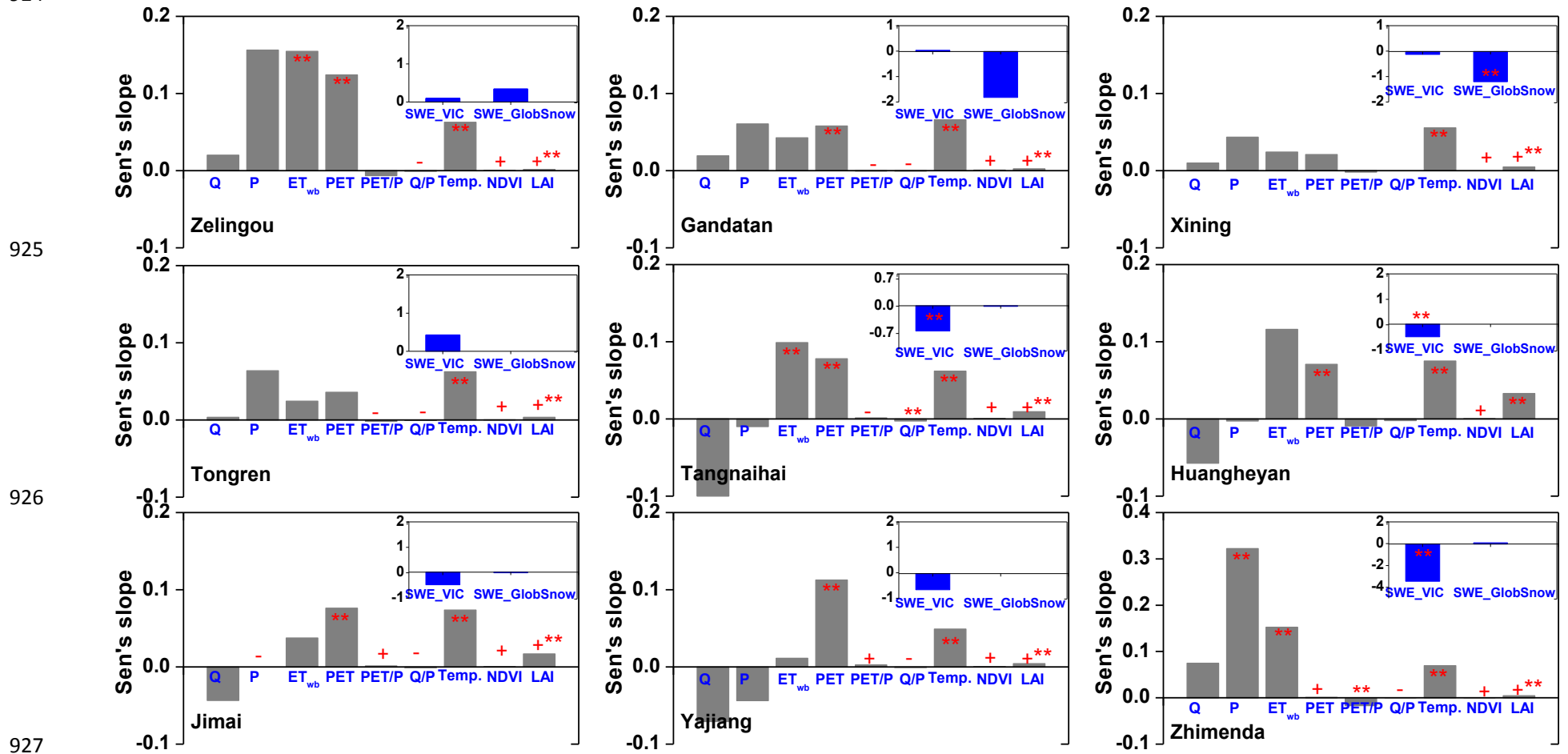


914  
 915

916 **Figure 9.** Linear and non-parametric trends of westerly, Indian monsoon and East Asian summer  
 917 monsoon during the period 1982-2011 revealed prospectively by the Asian Zonal Circulation  
 918 Index, Indian Ocean Dipole Mode Index and East Asian Summer Monsoon Index.



922 **Figure 10.** Similar to Figure 8 but for East Asian monsoon-dominated TP basins. It should be noted that the GlobSnow data are not available for some basins. The  
 923 double red stars showed that the trend was statistically significant at the 0.05 level.  
 924



930 **Figure 11.** Similar to Figure 8 but for Indian monsoon-dominated TP basins. It should be noted that the GlobSnow data are not available for some basins. The  
 931 double red stars showed that the trend was statistically significant at the 0.05 level.  
 932

